JPn Neuroscience
The Journal of Physiology

*J Physiol* 590.19 (2012) pp 4839–4858



# Sub- and suprathreshold adaptation currents have opposite effects on frequency tuning

Tara Deemyad[1,2], Jens Kroeger[1,2] and Maurice J. Chacron[1,2,3]

[1]*Department of Physiology,* [2]*Center for Applied Mathematics in Biology & Medicine and* [3]*Department of Physics, McGill University, Montreal, QC, Canada*

**Key points**

- We provide the first experimental evidence that sub- and suprathreshold adaptation currents, despite having similar effects on spike frequency adaptation, have opposite effects on frequency tuning.
- Through a combination of computational analysis and mathematical modelling, we reveal how the differential activation properties of these currents can lead to differential effects on the neuronal transfer function.
- Our findings challenge the common assumption that spike frequency adaptation always attenuates the neural response to low frequency stimuli, and instead suggest that spike frequency adaptation and frequency tuning can be regulated independently of one another.

**Abstract** Natural stimuli are often characterized by statistics that can vary over orders of magnitude. Experiments have shown that sensory neurons continuously adapt their responses to changes in these statistics, thereby optimizing information transmission. However, such adaptation can also alter the neuronal transfer function by attenuating if not eliminating responses to the low frequency components of time varying stimuli, which can create ambiguity in the neural code. We recorded from electrosensory pyramidal neurons before and after pharmacological inactivation of either calcium-activated ($I_{AHP}$) or KCNQ voltage-gated potassium currents ($I_M$). We found that blocking each current decreased adaptation in a similar fashion but led to opposite changes in the neuronal transfer function. Indeed, blocking $I_{AHP}$ increased while blocking $I_M$ instead decreased the response to low temporal frequencies. To understand this surprising result, we built a mathematical model incorporating each channel type. This model predicted that these differential effects could be accounted for by differential activation properties. Our results show that the mechanisms that mediate adaptation can either increase or decrease the response to low frequency stimuli. As such, they suggest that the nervous system resolves ambiguity resulting from adaptation through independent control of adaptation and the neuronal transfer function.

(Received 16 April 2012; accepted after revision 21 June 2012; first published online 25 June 2012)
**Corresponding author** M. J. Chacron: Department of Physiology, McGill University, 3655 Sir William Osler, room 1137, Montreal, QC, H3G 1Y6, Canada. Email: maurice.chacron@mcgill.ca

**Abbreviations** ELL, electrosensory lateral line lobe; SFA, spike frequency adaptation.

## Introduction

Natural stimuli are typically characterized by statistics that vary over orders of magnitude. In order to efficiently process these, sensory systems must continuously alter their response properties (Wark *et al.* 2007). Spike frequency adaptation (SFA), a relaxation of an initially high firing rate to a lower steady-state level following a sudden increase in stimulus intensity, is perhaps the most well-known example of such an alteration and is observed ubiquitously in the central nervous system (Sobel & Tank, 1994; Wang, 1998; Fuhrmann *et al.* 2002; Peron & Gabbiani, 2009*a*,*b*). It is clear that SFA can optimize coding of stimuli with changing statistics (Adorjan *et al.* 1999; Muller *et al.* 1999; Brenner *et al.* 2000; Fairhall *et al.* 2001; Dragoi *et al.* 2002; Ulanovsky *et al.* 2003; Benda


DOI: 10.1113/jphysiol.2012.234401

*et al.* 2005; Sharpee *et al.* 2006; Maravall *et al.* 2007). In addition, SFA introduces a high-pass filter to the neuronal transfer function (i.e. the relationship between response and temporal frequency), thereby attenuating (Nelson *et al.* 1997; French *et al.* 2001; Glantz & Schroeter, 2004; Benda *et al.* 2005) or completely eliminating (Benda & Hennig, 2008) the transmission of low frequency stimulus components including the mean. SFA can thus introduce ambiguity in the neural code as multiple stimuli with different statistics (e.g. mean) can then elicit the same neural response (e.g. firing rate) (Fairhall *et al.* 2001; Wark *et al.* 2007).

How does the central nervous system resolve such ambiguity? One possible solution to this problem is to have parallel and independent control of SFA and the neuronal transfer function. Parallel processing is a common strategy used across modalities including auditory (Takahashi *et al.* 1984; Oertel, 1999; Gelfand, 2004), visual (Marr, 1982; Livingstone & Hubel, 1987; Merigan & Maunsell, 1993), and electrosensory (Carr & Maler, 1986; Oswald *et al.* 2004; Bell & Maler, 2005; Kawasaki, 2005; McGillivray *et al.* 2012). However, while many mechanisms can lead to SFA (e.g. synaptic depression (Chance *et al.* 1998), inhibition (Wainwright *et al.* 2002), and calcium-activated small conductance (SK) (Williams *et al.* 1997; Smith *et al.* 2002; Hallworth *et al.* 2003) and M-type voltage-dependent (Adams *et al.* 1982; Halliwell & Adams, 1982) potassium channels that mediate $I_{AHP}$ and $I_M$ currents, respectively), how these affect the neuronal transfer function is poorly understood in general.

Here we investigated how $I_{AHP}$ and $I_M$ currents help shape the neuronal transfer function. To do so, we used the well-characterized electrosensory system of weakly electric fish. These fish sense perturbations of their self-generated electric field through an array of specialized electroreceptors on the skin that send projections to pyramidal neurons within the electrosensory lateral line lobe (Bell & Maler, 2005; Chacron *et al.* 2011). These pyramidal neurons benefit from well-characterized responses to sensory input (Maler, 2009), and express both SK and M channels (Ellis *et al.* 2007*b*, 2008; Deemyad *et al.* 2011). We applied the SK and M channel antagonists UCL-1684 (UCL) and XE-991 *in vitro*. While both antagonists caused increased excitability and attenuated spike frequency adaptation we found that they differentially affected the neuronal transfer function. Whereas UCL application increased the response to low frequency stimuli with respect to high frequency stimuli, XE-991 application decreased the response to low frequency stimuli with respect to high frequency stimuli. To better understand this result, we used an integrate-and-fire type model with both currents. Our model made important predictions about how the differential activation properties of $I_M$ and $I_{AHP}$ can explain their differential effects on frequency tuning. We then verified some of these predictions experimentally. Our results show for the first time that different mechanisms leading to SFA can have differential effects on the neuronal transfer function and suggest that SFA and frequency tuning can be regulated independently.

## Methods

### Animals

Male and female *Apteronotus leptorhynchus* specimens were purchased from tropical fish suppliers. These were acclimated and kept in the laboratory as per published guidelines (Hitschfeld *et al.* 2009). McGill University's Animal Care Committee approved all experimental and surgical procedures.

### Preparation of slices

Animals were anaesthetized by completely immersing them in a pH-adjusted MS-222 solution and then respirated via a mouth tube. Electrosensory lateral line lobe (ELL) slices (300–400 $\mu$m thickness) were then prepared using standard techniques (Mathieson & Maler, 1988; Ellis *et al.* 2007*b*) and were maintained by constant perfusion (2–3 ml min$^{-1}$) of artificial cerebrospinal fluid (ACSF; composition in mM: 126 NaCl, 2.5 KCl, 1.2 $NaH_2PO_4$, 1.2 $MgCl_2$, 18 $NaHCO_3$, 2.4 $CaCl_2$, and 11 D-glucose), as well as superfusion with carbogen (5% $CO_2$–95% $O_2$). The animals were killed by cervical dislocation during the surgery while anaesthetized.

### Recording procedures

Sharp intracellular recordings were made from the somata of ELL pyramidal neurons using glass microelectrodes that were pulled to a fine tip using a P-97 filament puller (Sutter Instrument Co., Novato, CA, USA) and filled with 2 M potassium acetate (Mathieson & Maler, 1988; Ellis *et al.* 2007*b*; Mehaffey *et al.* 2008*a*; Deemyad *et al.* 2011). Recordings were limited to electrosensory pyramidal neurons from the lateral segment of the ELL. This is because they display the greatest amount of SK channel expression (Ellis *et al.* 2008). Consequently, SK channel antagonists have the greatest effect on electrosensory pyramidal neuron activity within that segment (Ellis *et al.* 2007*b*; Deemyad *et al.* 2011). It is furthermore known that M channel antagonists such as XE-991 and linopirdine have a significant effect on electrosensory pyramidal neurons within that segment (Deemyad *et al.* 2011). An Axoclamp 900A (Molecular Devices, Sunnyvale, CA, USA) was used to amplify the recorded potential difference between the tip of the recording electrode and a ground wire placed in the bath, as well as to pass current through the recording electrode. Data were acquired at 10 kHz using a Digidata 1440A and Clampex 9.0 software (Molecular Devices). A holding

current was necessary to maintain the cell below spiking threshold (typically −0.3 nA). All current values reported hereafter are expressed relative to that holding current. The resting membrane potential did not change significantly throughout the recording of each neuron, which typically lasted for 1 h ($-72.45 \pm 2.07$ *vs.* $-71.37 \pm 2.29$, $n = 58$, paired $t$ test, $P = 0.2$). All pharmacological agents were dissolved in ACSF. UCL-1684 (Tocris Bioscience, Ellisville, MO, USA) (100 $\mu$M) was applied using a Picospritzer III (Parker Hannifin, Cleveland, OH, USA) to the ELL dorsal molecular layer by using patch electrodes with 1–2 $\mu$m tip diameter (Ellis *et al.* 2007*a*,*b*; Deemyad *et al.* 2011). XE-991 (Tocris) (7 $\mu$M) was bath applied as we observed that the drug took effect only after a long time (45 min), which is consistent with previous studies (Yue & Yaari, 2004; Deemyad *et al.* 2011).

## Stimulation and data analysis

All data analysis was performed in Matlab (The MathWorks, Nattick, MA, USA) using custom-written routines. Burst firing was quantified using the burst fraction (i.e. the fraction of interspike intervals whose value is less than 10 ms) (Oswald *et al.* 2004; Ellis *et al.* 2007*a*,*b*; Avila Akerberg & Chacron, 2011). The spike times were defined as the times for which the membrane potential crossed a suitable threshold (typically −30 mV) from below. The medium afterhyperpolarization (AHP) was measured as the difference between the average membrane potential values 10–15 ms before and 10–40 ms after the action potential peak (Faber & Sah, 2002; Koyama & Appel, 2006; Deemyad *et al.* 2011).

**Spike frequency adaptation.** Spike frequency adaptation (SFA) was characterized by first computing the peri-stimulus time histogram (PSTH) with 15 ms bin width in response to a 300 ms duration depolarizing current step of 0.3 nA that was repeated 100 times with 1.7s interval between successive presentations. The PSTH was then normalized by its maximum value and the adaptation time constant was obtained by fitting a decaying exponential function. We note that this normalization does not alter the value of the activation time constant obtained.

**Subthreshold input resistance and membrane time constant.** The subthreshold input resistance was measured from Ohm's law. We used the change in voltage resulting from a −0.4 nA current step that was 300 ms in duration while the membrane time constant was obtained by fitting a decaying exponential function to the membrane potential trace as was done previously (Ellis *et al.* 2007*a*; Deemyad *et al.* 2011).

**Positive step current injections.** We used a set of 10 current steps, each lasting 1 s and ranging from 0.05 to 0.5 nA above the baseline holding current. We plotted the mean firing rate as a function of the current value (*f–I*) curve. The gain and rheobase (i.e. the minimum current needed to elicit spiking activity) were determined from the slope and $x$-intercept of the best linear fit to the *f–I* curve for current values that gave rise to action potential firing (i.e. greater or equal than rheobase), respectively (Mehaffey *et al.* 2005; Deemyad *et al.* 2011).

**Neuronal transfer function.** We quantified the neural transfer function from the spiking response to low-pass filtered (120 Hz cutoff, 8th order Butterworth filter) white noise currents with duration 90 s, mean value 0.25 nA and standard deviation 0.2 nA that were injected through the recording electrode. This broadband noise is meant to mimic the signals that a fish encounters in the presence of nearby conspecifics (Tan *et al.* 2005; Stamper *et al.* 2010) and has been used previously to quantify the frequency tuning of electrosensory pyramidal neurons both *in vitro* (Oswald *et al.* 2004; Ellis *et al.* 2007*a*; Mehaffey *et al.* 2008*b*) and *in vivo* (Krahe *et al.* 2008). The standard deviation of the noise was adjusted such as to give membrane potential fluctuations that are comparable to those seen *in vivo* in response to sensory input as done previously (Deemyad *et al.* 2011) (Fig. 1*A*). A binary sequence $R(t)$ with a bin width $\mathrm{d}t$ of 0.5 ms was then constructed from the spike times $t_i$ in response to the noise current injection by setting the content of bin $i$ to 1 if there is one spike time $t_j$ such that $i \times \mathrm{d}t \leq t_j \leq (i+1) \times \mathrm{d}t$ and 0 otherwise. Note that, since $\mathrm{d}t$ is below the absolute refractory period of electrosensory pyramidal cells (1–2 ms, (Berman & Maler, 1998)), there can be at most one spike time within any given bin.

The neuronal transfer function was quantified using the response gain $G(f) = |P_{rs}(f)|/P_{ss}(f)$. Here $P_{rs}(f)$ denotes the cross spectrum between the stimulus $S(t)$ and the response $R(t)$ while $P_{ss}(f)$ is the power spectrum of the stimulus $S(t)$. Because we were interested in the relative shape of the gain curve (e.g. low-pass, high-pass, band-pass), the gain was normalized by its value at 50 Hz. We also quantified the neuronal transfer function by computing the mutual information rate density (i.e. the mutual information rate as a function of frequency) between the binary sequence $R(t)$ and the noise stimulus using (Rieke *et al.* 1996; Borst & Theunissen, 1999; Chacron *et al.* 2003*b*):

$$I(f) = -log_2 [1 - C(f)] / f_r. \quad (1)$$

The mutual information rate density is expressed in bits spike$^{-1}$ Hz$^{-1}$. Here $f_r$ is the mean firing rate during stimulation and $C(f)$ is the coherence function at temporal frequency $f$ which is given by:

$$C(f) = \frac{|P_{rs}(f)|^2}{P_{rr}(f) P_{ss}(f)}, \quad (2)$$

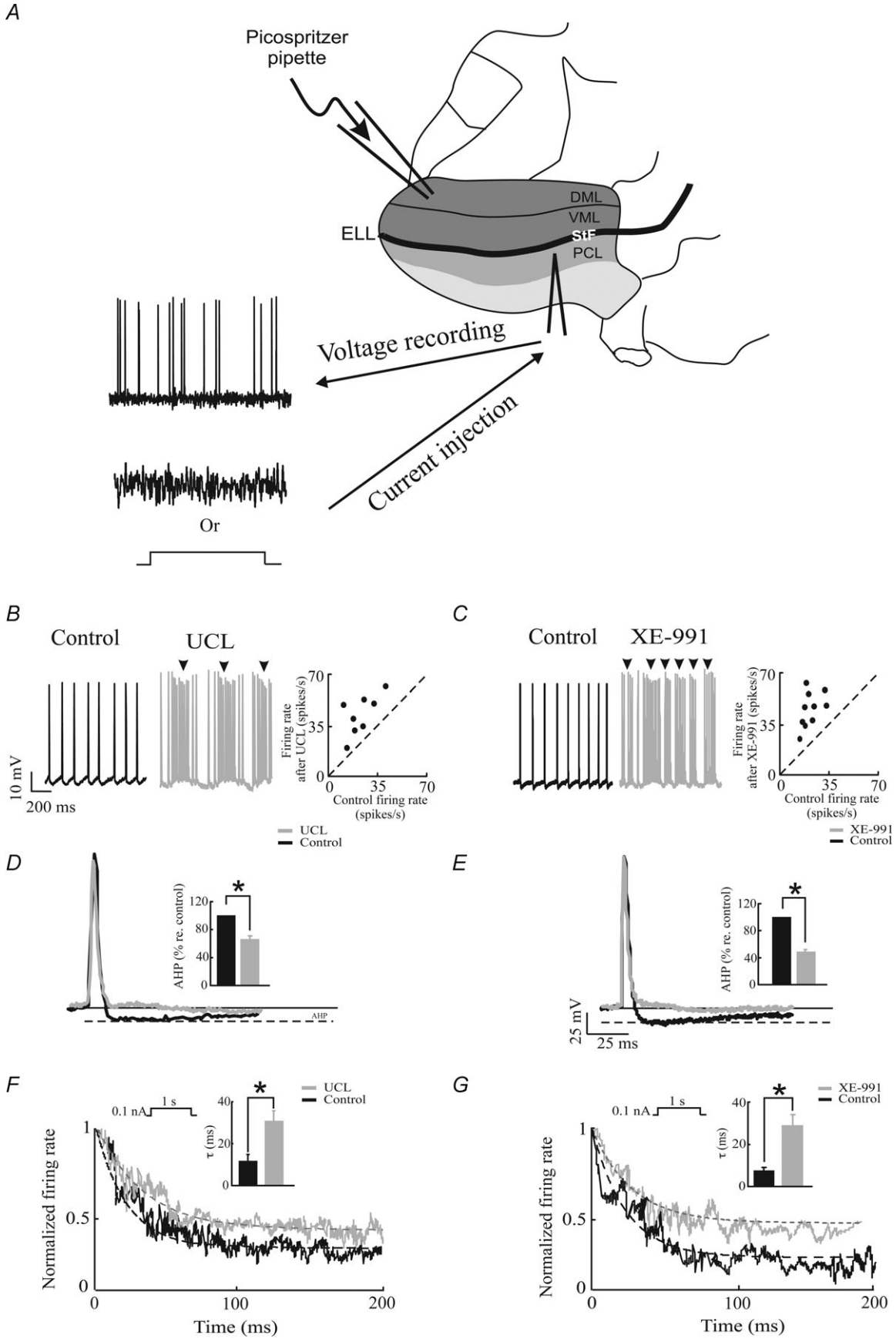

where $P_{rs}(f)$ denotes the cross spectrum between $S(t)$ and $R(t)$, $P_{ss}(f)$ is the power spectrum of the stimulus $S(t)$, and $P_{rr}(f)$ is the power spectrum of the binary sequence $R(t)$. We then normalized the mutual information by its value at 50 Hz. We note that we used both measures as they can give rise to qualitatively different results (Chacron *et al.* 2005*b*; Sadeghi *et al.* 2007; Lindner *et al.* 2009). We then computed the tuning index from both the gain and mutual information curves as the ratio of the average values for low (0–40 Hz) and high (80–120 Hz) frequencies.

### Pyramidal cell classification

There are two types of electrosensory pyramidal neurons: basilar and non-basilar pyramidal cells. Basilar and non-basilar pyramidal neurons can be distinguished anatomically based on the presence/absence of a basilar bush, respectively (Maler, 1979; Maler *et al.* 1981), as well as their responses to broadband noise current injection *in vitro* (Mehaffey *et al.* 2008*b*; Deemyad *et al.* 2011). Indeed, previous studies have shown that cells with tuning index less than 0.5 are of the basilar type while cells with tuning index greater than 0.5 are of the non-basilar type (Deemyad *et al.* 2011). This criterion was used to distinguish between basilar and non-basilar pyramidal cells in this study.

As previous studies have shown that SK channel antagonists have no significant effect on non-basilar cells (Ellis *et al.* 2007*b*; Deemyad *et al.* 2011), we only included basilar pyramidal cells in the dataset for which UCL was applied. We note that the lack of an effect correlates with the absence of expression of SK channels near the somata of non-basilar pyramidal cells (Ellis *et al.* 2007*b*, 2008), and is thus not indicative that the drug is not effective in the electrosensory system. In contrast, the M channel antagonist XE-991 was previously shown to have a significant effect on both basilar and non-basilar pyramidal cells (Deemyad *et al.* 2011). As such, we included both basilar and non-basilar pyramidal cells in the dataset for which XE-991 was applied. Although the neuronal transfer functions of basilar and non-basilar pyramidal cells differed significantly, which is consistent with previous results (Ellis *et al.* 2007*b*; Mehaffey *et al.* 2008*b*), we found that XE-991 affected their tuning in a similar fashion. As such, the data from both cell types were pooled.

### Statistical analysis

Statistical significance was assessed by Student's $t$ test. All values are reported in the text as means ± SEM. Differences were deemed to be statistically significant if $P < 0.05$ and are reported by an asterisk in the figures.

### Modelling

We used a model based on the integrate-and-fire formalism with subthreshold and spike-triggered adaptation currents. Such models have been previously considered and shown to reproduce experimental data (Chacron *et al.* 2001*b*,*a*; Brette & Gerstner, 2005; Naud *et al.* 2008; Walcott *et al.* 2011). The model has eight parameters: capacitance $C_m$, leak conductance $g_{leak}$, leak reversal potential $E_{leak}$, threshold potential $V_T$, reset potential $Vr$, activation time constant $\tau_w$, subthreshold adaptation gain $a$, and spike-triggered adaptation gain $b$. The parameters determine temporal evolution of membrane potential $V_m$ and adaptation current $w$, according to the following equations:

$$C_m \frac{dV_m}{dt} = -g_{leak}(V_m - E_{leak}) - w + I_{bias} + s(t) + \xi(t) \quad (3)$$

$$\tau_w \frac{dw}{dt} = a\, w_\infty(V_m) - w + b\, \tau_w \sum_{i=1}^{N} \delta(t - t_i), \quad (4)$$

**Figure 1. UCL and XE-991 application give rise to similar changes in membrane excitability and SFA**
*A*, schematic diagram of the experimental set-up. Sharp intracellular recordings were made from electrosensory pyramidal neurons and the spiking responses to step or noise current injection were obtained under control conditions or after UCL or XE-991 application. DML: dorsal molecular layer; VML: ventral molecular layer; PCL: pyramidal cell layer; StF: stratum tractus fibrosum; ELL: electrosensory lateral line lobe. *B*, membrane potential trace from a typical electrosensory pyramidal neuron before (left) and after UCL application (middle). Note the bursting activity (arrows). The firing rate after UCL application is plotted as a function of the firing rate under control conditions (right). *C*, same as *B*, but with XE-991 application. *D*, action potential shapes for control (black) and after UCL application (grey). Inset, population-averaged AHP size under control and after UCL application. *E*, same as *D* but for XE-991 application. *F*, peri-stimulus time histogram (PSTH) before (black) and after (grey) UCL application with fitted exponential decay curves (dashed lines). Inset, population averaged adaptation time constants before and after UCL application. It is seen that UCL application significantly increases the activation time constant. *G*, same as *F* but for XE-991 application. *Statistical significance at the $P = 0.01$ using a pairwise $t$ test.

where $I_{bias}$ is a bias current, $s(t)$ is the stimulus which is low-pass filtered (120 Hz cutoff, 8th order Butterworth) Gaussian white noise with zero mean and standard deviation $\sigma_s$, $\xi(t)$ is Gaussian white noise with zero mean and standard deviation $\sigma_n$, $\delta(t)$ is the delta function, and $w_\infty(V_m)$ is a sigmoidal function given by:

$$w_\infty(V_m) = \frac{1}{1 + exp\left[-\frac{V_m+70}{4}\right]}. \quad (8)$$

We note that eqn (4) differs from the expression used in previous studies (Brette & Gerstner, 2005; Naud *et al.* 2008; Walcott *et al.* 2011) as we have introduced a sigmoidal dependency on the activation of the subthreshold adaptation current – this is meant to mimic the nonlinear dependence of subthreshold adaptation currents on membrane voltage seen experimentally (Madamba *et al.* 1999). In particular, we note that this implies that the subthreshold adaptation current is non-zero at $V_m = -70$ mV. Every time $V_m$ exceeds a threshold of $V_T = -40$ mV, is it instantaneously set to $V_{max} = 20$ mV, reset to $V_r = -70$ mV, and an action potential is said to have occurred. The adaptation current is then incremented by an amount $b$. Other parameter values used were, unless otherwise specified, $I_{bias} = 0.3$ nA, $\sigma_s = 0.3$ nA, $\sigma_n = 0.5$ nA, $g_{leak} = 0.02$ $\mu$S, $C_m = 0.1$ nF, $\tau_w = 10$ ms, $E_{leak} = -70$ mV. These values were chosen based on available experimental data (Krahe *et al.* 2008; Prescott & Sejnowski, 2008; Toporikova & Chacron, 2009), or were systematically varied, or were chosen such as to make the model's output consistent with our experimental results. We mimicked the effects of SK and M channel blocking by setting the spike-triggered adaptation and subthreshold adaptation gains $b$ and $a$, respectively, to 0. Finally, we note that our simple model does not include all the other voltage-gated conductances as well as the known spatial extent of ELL pyramidal cells. This is because our model was thus not designed to reproduce all the known features of ELL pyramidal cells. Rather, it was designed to help us understand in general how sub- and suprathreshold adaptation currents can affect the neuronal transfer function. The equations were integrated with Matlab using an Euler–Maruyama algorithm with a time step of 0.025 ms.

### Approximating the behavior of the subthreshold adaptation current

We derive approximate expressions for the subthreshold adaptation current $w$ (i.e. $b = 0$ nA) in the limit of low and high values of $\tau_w$. In the limit $\tau_w \to 0$, we have $w \approx a w_\infty(V)$. Putting this in eqn (3) and expanding $w_\infty(V_m)(V_m - E_{leak})$ in a Taylor series to first order around $V_m = E_{leak}$ gives:

$$C_m \frac{dV_m}{dt} \approx -g_{leak}(V_m - E_{leak}) - \frac{a}{16}(V_m - E_{leak}) - \frac{a}{2} + I_{bias} + s(t) + \xi(t) \quad (6)$$

$$= -\left(g_{leak} + \frac{a}{16}\right)(V_m - E_{leak}) + I_{bias} + s(t) + \xi(t), \quad (7)$$

where we have neglected the term $a/2$, which is valid in the limit of high values of $I_{bias}$. This expression shows that decreasing the subthreshold adaptation gain $a$ is mathematically equivalent to decreasing the leak conductance $g_{leak}$ in the limit of small activation time constant $\tau_w$.

In the limit $\tau_w \to \infty$, we can replace $w$ by its average, $<w>$, in eqn (3), which gives:

$$C_m \frac{dV_m}{dt} \approx -g_{leak}(V_m - E_{leak}) - \langle w \rangle + I_{bias} + s(t) + \xi(t). \quad (8)$$

As such, decreasing the subthreshold adaptation gain $a$ is instead mathematically equivalent to increasing the bias current $I_{bias}$ in the limit of large activation time constant $\tau_w$.

## Results

We recorded intracellularly from 58 ELL pyramidal neurons (with about 60% being E-cells) *in vitro* in 28 fish while giving current injection through the recording electrode. This current injection consisted of steps as well as broadband (0–120 Hz) Gaussian noise (Fig. 1*A*). The responses to these stimuli were accumulated under control conditions and after application of either UCL or XE-991.

### Effects of UCL and XE-991 application on pyramidal neuron excitability and SFA

We first quantified the effects of UCL and XE-991 application on pyramidal neuron excitability. We found that pyramidal neurons responded with tonic firing to positive current step injections under control conditions (Figs 1*B* and *C*). In contrast, we found that these same neurons tended to respond with bursts (i.e. clusters of action potentials followed by quiescence) in response to the same depolarizing current steps after applying either UCL (Fig. 1*B*, arrows) or XE-991 (Fig. 1*C*, arrows). Indeed, both UCL and XE-991 application significantly increased the burst fraction (i.e. the fraction of interspike intervals that are less than 10 ms) (UCL: ~650 ± 56% increase re. control, paired $t$ test, $P = 0.02$, $n = 6$; XE-991: ~600 ± 120% increase re. control, paired $t$ test,

$P = 0.01$, $n = 6$). This increased tendency to fire bursts of action potentials was accompanied by a strong and significant reduction in the afterhyperpolarization (AHP) following each action potential (UCL: $65.78 \pm 5.8\%$ re. control; $P = 0.01$, paired $t$ test, $n = 6$; XE-991: $48.22 \pm 3.07\%$ re. control; $P = 0.03$, paired $t$ test, $n = 6$) (Fig. 1*D* and *E*). Finally, both UCL and XE-991 application caused significant increases in firing rate (UCL application; control: $22.9 \pm 4.2$ Hz; UCL: $45.8 \pm 5.6$ Hz, paired $t$ test, $P = 0.01$, $n = 8$; XE-991 application; control: $19.0 \pm 1.3$ Hz; XE-991: $44.4 \pm 5.3$ Hz, paired $t$ test, $P = 0.0001$, $n = 10$) (Fig 1*C*).

We next characterized the effects of UCL and XE-991 application on SFA. Our results show that UCL and XE-991 application both decreased SFA (Fig. 1*F* and *G*, respectively). This decrease was quantified using the adaptation time constant. UCL application significantly increased the adaptation time constant (control: $11.6 \pm 2.99$ ms; UCL: $30.80 \pm 4.91$ ms, paired $t$ test, $P = 0.02$, $n = 6$) (Fig. 1*F*). We found that XE-991 application also significantly increased the adaptation time constant (control: $7.40 \pm 1.83$ ms; XE-991: $28.70 \pm 5.40$ ms, paired $t$ test, $P = 0.01$, $n = 6$ respectively) (Fig. 1*G*, insets).

## Effects of UCL and XE-991 application on pyramidal neuron transfer function

We next characterized the effects of UCL and XE-991 application on the neuronal transfer function as quantified by gain and mutual information density curves. To do so, we recorded the spiking responses of electrosensory pyramidal neurons to broadband noise current injection under control conditions and after application of either UCL or XE-991. We found that UCL application significantly altered the neuronal transfer function in that it increased the response to the low frequency (<40 Hz) stimulus components relative to high frequencies. This was observed for both the gain (Fig. 2*A* and *B*) and the mutual information density (Figs 2*C* and *D*) measures. We quantified this change by computing a tuning index and found that UCL application significantly increased the tuning index for both the gain (change re. control: $119 \pm 3\%$, paired $t$ test, $P = 0.01$, $n = 7$; Fig. 2*A*, inset) and mutual information density (change re. control: $190 \pm 21\%$, paired $t$ test, $P = 0.01$, $n = 7$; Fig. 2*C*, inset) curves.

XE-991 application also significantly altered the neuronal transfer function, but in a qualitatively different manner. Indeed, XE-991 application instead decreased the response to the low frequency (<40 Hz) stimulus components relative to high frequencies. This was observed for both the gain (Fig. 2*E* and *F*) and the mutual information density (Fig. 2*G* and *H*) measures. We also quantified this change by computing the tuning index and found that XE-991 application significantly decreased the tuning index for both the gain (change re. control: $79 \pm 8\%$, paired $t$ test, $P < 0.001$ $n = 10$; Fig. 2*E*, inset) and the mutual information density (change re. control: $73 \pm 14\%$, paired $t$ test, $P = 0.02$, $n = 10$; Fig. 2*G*, inset).

## UCL and XE-991 application have differential effects on the steady state *f–I* curve

How can the opposite effects of UCL and XE-991 application on the neuronal transfer function be explained? Theoretical studies predict that the effects of SFA on the neuronal transfer for low frequencies can be inferred from its effects on the steady state firing rate *vs.* constant current injected (i.e. *f–I*) curve (Benda & Herz, 2003). As such, we first characterized the effects of UCL and XE-991 application on the steady state *f–I* curve.

We found that UCL application significantly altered the *f–I* curve by increasing its slope (i.e. the gain) (change re. control: $50 \pm 15\%$, paired $t$ test, $P = 0.02$, $n = 7$) but without changing the rheobase current value (i.e. the minimum current value needed to elicit action potential firing) (change re. control: $0.06 \pm 0.09$ nA, paired $t$ test, $P = 0.4$, $n = 7$) (Fig. 3*A*). In contrast, XE-991 application altered the *f–I* curve in a qualitatively different manner as it significantly decreased the rheobase current (change re. control: $-0.19 \pm 0.08$ nA, paired $t$ test, $P = 0.03$, $n = 7$) without changing its slope (change re. control $15 \pm 30\%$, paired $t$ test, $P = 0.9$, $n = 7$) (Fig. 3*B*).

Theoretical studies predict that changes in the *f–I* curve slope obtained for constant current injection can explain changes in the gain for low frequencies obtained under noise current injection (Benda & Herz, 2003). We thus tested this prediction experimentally by plotting the predicted change in gain (i.e. the value of *f–I* curve slope under control conditions minus the value after either UCL or XE-991 application) as a function of the actual change in gain (i.e. the value of gain at zero frequency under control conditions minus the value after either UCL or XE-991 application) for our dataset. For UCL application, we found a strong and significant positive correlation ($R = 0.8$, $P = 0.01$, $n = 7$) (Fig. 3*C*). In contrast, for XE-991 application, we found no significant correlation ($R = 0.25$, $P = 0.41$, $n = 12$) (Fig. 3*D*).

## UCL and XE-991 differentially affect subthreshold membrane properties

Thus far, our results have shown that UCL and XE-991 application gave rise to similar changes in neural excitability but also gave rise to qualitatively different changes in the neuronal transfer function and the steady state *f–I* curve. While we have found that the changes in the

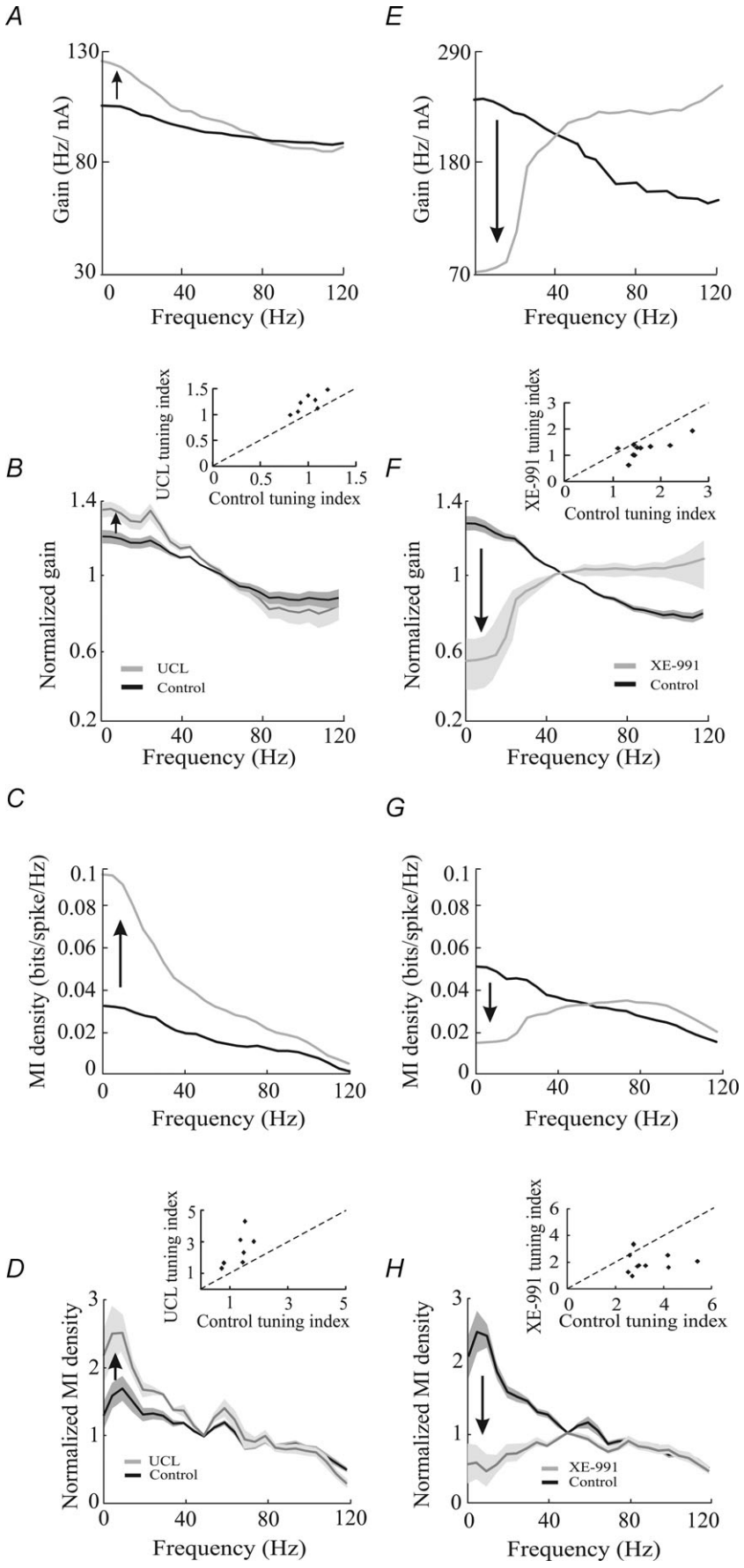


**Figure 2. UCL and XE-991 application give rise to opposite changes in the neuronal transfer function**
*A*, gain curves before (black) and after (grey) UCL application from a typical E-type electrosensory pyramidal neuron. *B*, normalized population-averaged gain curves before (black) and after (grey) UCL application. The bands indicate 1 SEM. Inset, scatter plot showing tuning index values obtained after UCL application as a function of those obtained under control conditions. *C*, mutual information (MI) density curves for the same example neuron before (black) and after (grey) UCL application from this same neuron. *D*, normalized population-averaged MI density curves before (black) and after (grey) UCL application. The bands indicate 1 SEM. Inset, scatter plot showing tuning index values obtained after UCL application as a function of those obtained under control conditions. *E*, gain curves before (black) and after (grey) XE-991 application from a typical I-type electrosensory pyramidal neuron. *F*, normalized population-averaged gain curves before (black) and after (grey) XE-991 application. The bands indicate 1 SEM. Inset, scatter plot showing tuning index values obtained after XE-991 application as a function of those obtained under control conditions. *G*, MI density curves before (black) and after (grey) XE-991 application from the same example neuron. *H*, population-averaged normalized MI density curves before (black) and after (grey) XE-991 application. The bands indicate 1 SEM. Inset, scatter plot showing tuning index values obtained after XE-991 application as a function of those obtained under control conditions. *Statistical significance at the $P = 0.01$ using a pairwise *t* test.

neuronal transfer function and *f–I* curve were consistent for UCL application, these changes were not consistent for XE-991 application.

We next explored whether UCL and XE-991 application gave rise to changes in the subthreshold membrane properties such as resistance and time constant. Based on results obtained in other systems, we would predict that XE-991 application increases both the subthreshold membrane resistance and the membrane time constant. This is because voltage-dependent M channels can be activated at transmembrane potentials below those that elicit action potential firing (i.e. they are activated in the subthreshold regime) (Sogaard *et al.* 2001; Shah *et al.* 2002; Yue & Yaari, 2004). In contrast, SK channel activation

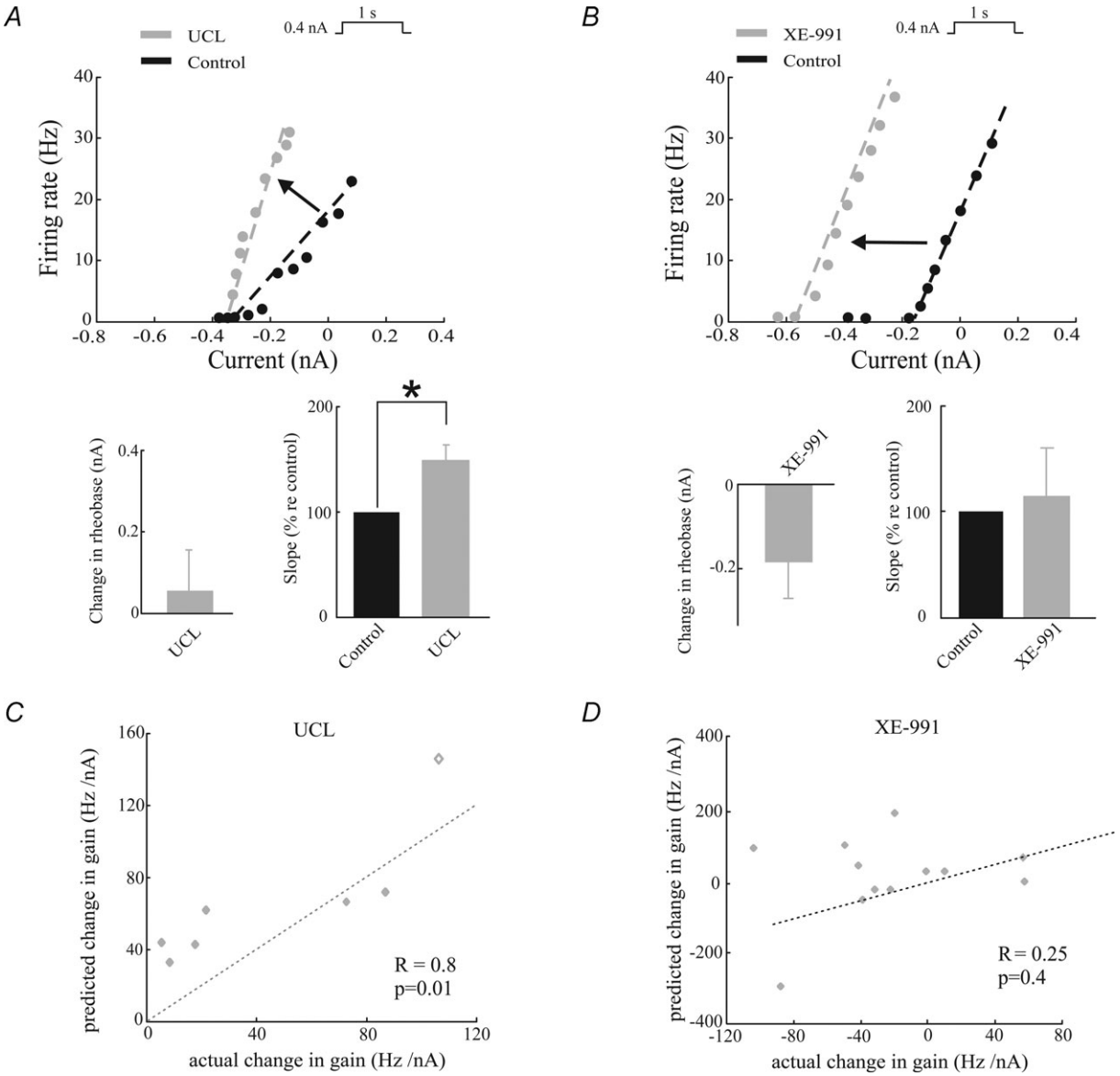


**Figure 3. UCL and XE-991 application give rise to differential changes on the frequency as a function of current (*f–I*) curve**

*A*, top, *f–I* curves before (black) and after (grey) UCL application from a typical electrosensory pyramidal neuron. Bottom left, population-averaged change in rheobase. Bottom right, population-averaged *f–I* curve slope values before and after UCL application. *B*, same as *A*, but for XE-991 application. The dashed lines were obtained by performing a linear least squares fit on the data points for which the firing rate was strictly positive. *C*, change in *f–I* curve slope (i.e. the predicted change in gain) as a function of the actual change in gain computed from time varying stimuli evaluated at zero frequency. A significant positive correlation is observed with ($R = 0.8$, $P = 0.01$, $n = 7$) and without ($R = 0.73$, $P = 0.03$, $n = 6$) the data point shown as a diamond. The dashed line is the identity line. *D*, same as *C*, but for XE-991 application. No significant correlation was observed ($R = 0.25$, $P = 0.41$, $n = 12$).

does not explicitly depend on the transmembrane voltage but instead depends solely on the intracellular calcium concentration (Sah & Faber, 2002). As previous studies have shown that this concentration can increase both in the sub- and suprathreshold (i.e. spiking) regimes, SK channels can *a priori* be activated in both regimes (Faber & Sah, 2003). As such, UCL application may or may not increase the subthreshold membrane resistance and time constant.

We measured the subthreshold membrane resistance by holding pyramidal neurons below the spiking threshold and injecting a negative current step. We found that the voltage responses to such steps were almost identical under control conditions and after UCL application (Fig. 4*A*). Indeed, both the subthreshold membrane resistance (control: $12.87 \pm 6.08$ MΩ; UCL: $12.94 \pm 3.97$ MΩ, paired $t$ test, $P = 0.9$, $n = 5$) and the membrane time constant (control: $16.21 \pm 1.70$ ms *vs.* UCL: $19.15 \pm 2.10$ ms, paired $t$ test, $P = 0.9$, $n = 5$) were not significantly altered by UCL application.

In contrast, we found that the voltage deflection in response to a negative current step was greater after XE-991 application (Fig. 4*B*). Indeed, both the subthreshold membrane resistance (control: $13.67 \pm 3.08$ MΩ; XE-991: $23.5 \pm 2.83$ MΩ, paired $t$ test, $P = 0.002$, $n = 5$) and time constant (control: $16.66 \pm 2.60$ ms *vs.* XE-991: $42.16 \pm 4.60$ ms, paired $t$ test, $P = 0.02$, $n = 5$) were significantly increased. Further, we found that, while UCL application did not significantly alter the resting membrane potential value (control: $-72.6 \pm 2.1$ mV,

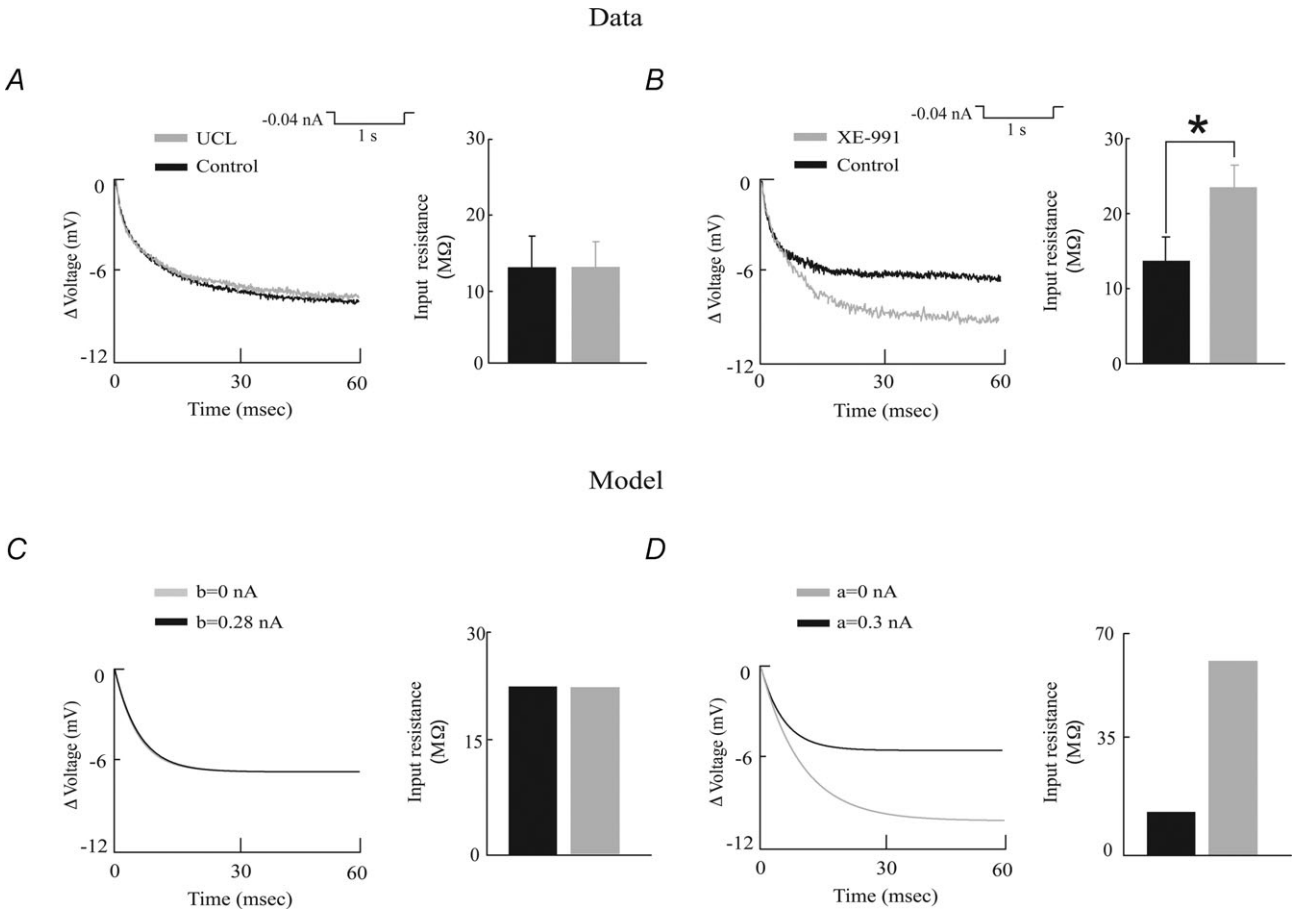


**Figure 4. UCL and XE-991 application differentially affect the subthreshold membrane resistance**
*A*, left, membrane potential trace in response to a hyperpolarizing current step before (black) and after (grey) UCL application. Inset, population-averaged input resistances before and after UCL application. *B*, left, membrane potential trace in response to a hyperpolarizing current step before (black) and after (grey) XE-991 application. Inset, population-averaged input resistances before and after XE-991 application. *C*, model membrane potential trace under control conditions (black) and after removing the spike-triggered adaptation current (grey). Right, corresponding model input resistances. Parameter values were $\tau_w = 10$ ms, $I_{bias} = 0.35$ nA, $g_{leak} = 0.018$ $\mu$S, $a = 0$ nA, and $b = 0.28$ nA (black) and 0 (grey). *D*, model membrane potential trace under control conditions (black) and after removing the subthreshold adaptation current (grey). Right, corresponding model input resistances. Parameter values were $\tau_w = 100$ ms, $I_{bias} = 0.35$ nA, $g_{leak} = 0.02$ $\mu$S, $b = 0$ nA, and $a = 0.3$ nA (control) and 0 (grey). *Statistical significance at the $P = 0.01$ level using a pairwise $t$ test.

UCL: $-71.2 \pm 2.2$ mV, paired $t$ test, $P = 0.16$, $n = 7$), XE-991 application instead led to a significant increase (control: $-74.6 \pm 4.9$ mV, XE-991: $-72.0 \pm 5.0$ mV, paired $t$ test, $P = 0.01$, $n = 12$).

## Modelling

Could the differential effects of UCL and XE-991 application on subthreshold membrane properties explain their differential effects on the neuronal transfer function? We explored this possibility by building a mathematical model based on the integrate-and-fire formalism that includes subthreshold and spike-triggered adaptation currents. Such models have been previously shown to accurately reproduce experimental data despite their apparent simplicity (Brette & Gerstner, 2005; Naud *et al.* 2008; Walcott *et al.* 2011). Parameter values were either systematically varied or chosen based on available data (Krahe *et al.* 2008; Prescott & Sejnowski, 2008; Toporikova & Chacron, 2009).

**Model validation.** We then validated our model against our existing experimental data. To do so, we first tested that removing the subthreshold and spike-triggered adaptation currents from our model gave rise to qualitatively similar effects on subthreshold membrane resistance and time constant. To do so, we simulated our model's transmembrane potential response to a negative current step as in the experimental data. Consistent with our experimental data, we found that our model's response to a negative current step was unchanged after removing the spike-triggered adaptation current by setting its gain $b$ to zero (Fig. 4*C*), which is indicative that the subthreshold membrane resistance is unchanged. This was also true for the membrane time constant (10 ms). We also found that, after removing the subthreshold adaptation current by setting its gain $a$ to zero, our model responded to a negative current step with a greater hyperpolarization (Fig. 4*D*), which is indicative of an increased subthreshold membrane resistance. The membrane time constant also increased (10 ms to 18.1 ms).

We next tested whether our model could reproduce the effects of UCL and XE-991 application on excitability that were observed experimentally. We found that our model neuron responded to positive step current injections with tonic firing under control conditions (i.e. when either the subthreshold or the spike-triggered adaptation currents were included) (Fig. 5*A* and *B*, left panels). Simulating UCL and XE-991 application by setting the spike-triggered and subthreshold adaptation gains, $b$ and $a$, to zero, respectively, caused increased activity as observed experimentally (Fig. 5*A* and *5B*, right panels). Indeed, the mean firing rate increased from 14.85 Hz to 41.19 Hz and from 9.25 Hz to 41.19 Hz when we set $a$ and $b$ to zero, respectively. This increased activity was accompanied by a decreased AHP (Fig. 5*C* and *D*).

Finally, we tested whether our model could reproduce the effects of UCL and XE-991 application on the steady state *f–I* curves. Increasing the spike-triggered adaptation gain $b$ decreased the *f–I* curve slope without changing the rheobase (Fig. 5*E*). In contrast, increasing the subthreshold adaptation gain $a$ increased the rheobase without changing the *f–I* curve slope (Fig. 5*F*).

**Simulating the effects of UCL on the neuronal transfer function.** Since we found that our model could qualitatively reproduce our experimental results so far, we next computed the neuronal transfer function under control conditions and after simulating UCL application. We found that increasing the spike-triggered adaptation current gain $b$ gave rise to decreased gain at low (<30 Hz) frequencies (Fig. 6*A*). We then systematically varied both the spike-triggered adaptation gain $b$ and the bias current $I_{bias}$ and computed the tuning index as well as firing rate. We found that, for a fixed value of $I_{bias}$, increasing $b$ decreased the tuning index (Fig. 6*B*) and the firing rate (Fig. 6*C*). We note that qualitatively similar results were obtained using the mutual information density measure and by varying the activation time constant $\tau_w$ (data not shown).

**Simulating the effects of XE-991 on the neuronal transfer function.** As experimental results have shown that the activation time constants of subthreshold KCNQ channels vary over a wide range (10–500 ms) (Sogaard *et al.* 2001; Prole *et al.* 2003; Regev *et al.* 2009), we next investigated the effects of changing the subthreshold adaptation gain $a$ as well as its activation time constant $\tau_w$ on the neuronal transfer function. We found that, for high values of $\tau_w$, increasing $a$ led to an increased gain at low (<30 Hz) frequencies relative to high frequencies (Fig. 7*A*). We then computed the tuning index and firing rate as a function of both the subthreshold adaptation gain $a$ and the bias current $I_{bias}$ and observed that, for a fixed value of $I_{bias}$, increasing $a$ decreased the tuning index (Fig. 7*B*) and the firing rate (Fig. 7*C*).

However, qualitatively different results were obtained for low values of $\tau_w$. Indeed, we found that increasing $a$ decreased the gain at low frequencies (Fig. 7*D*). We then computed the tuning index and firing rate as a function of both the subthreshold adaptation gain $a$ and the bias current $I_{bias}$ and observed that, for a fixed value of $I_{bias}$, increasing $a$ now increased the tuning index (Fig. 7*E*). We note that, for a fixed value of the bias current $I_{bias}$, increasing $a$ still led to a decrease in firing rate (Fig. 7*F*) that was similar to that obtained for high values of the activation time constant $\tau_w$ (compare Figs. 7*C* and *F*).

To better illustrate how increasing the subthreshold adaptation gain $a$ can differentially affect the neuronal transfer function depending on the value of the activation time constant $\tau_w$, we next computed the tuning index as a function of both the subthreshold adaptation current gain $a$ and the time constant $\tau_w$ (Fig. 8*A*). We found that increasing $a$ decreases the tuning index for low values of $\tau_w$ and increases it for high values of $\tau_w$. However, increasing $a$ always decreases firing rate regardless of the value of $\tau_w$ used (Fig. 8*B*).

**Explaining the effects of XE-991 on the neuronal transfer function.** We next sought to explain why the subthreshold adaptation had differential effects on the neuronal transfer function depending on the value of

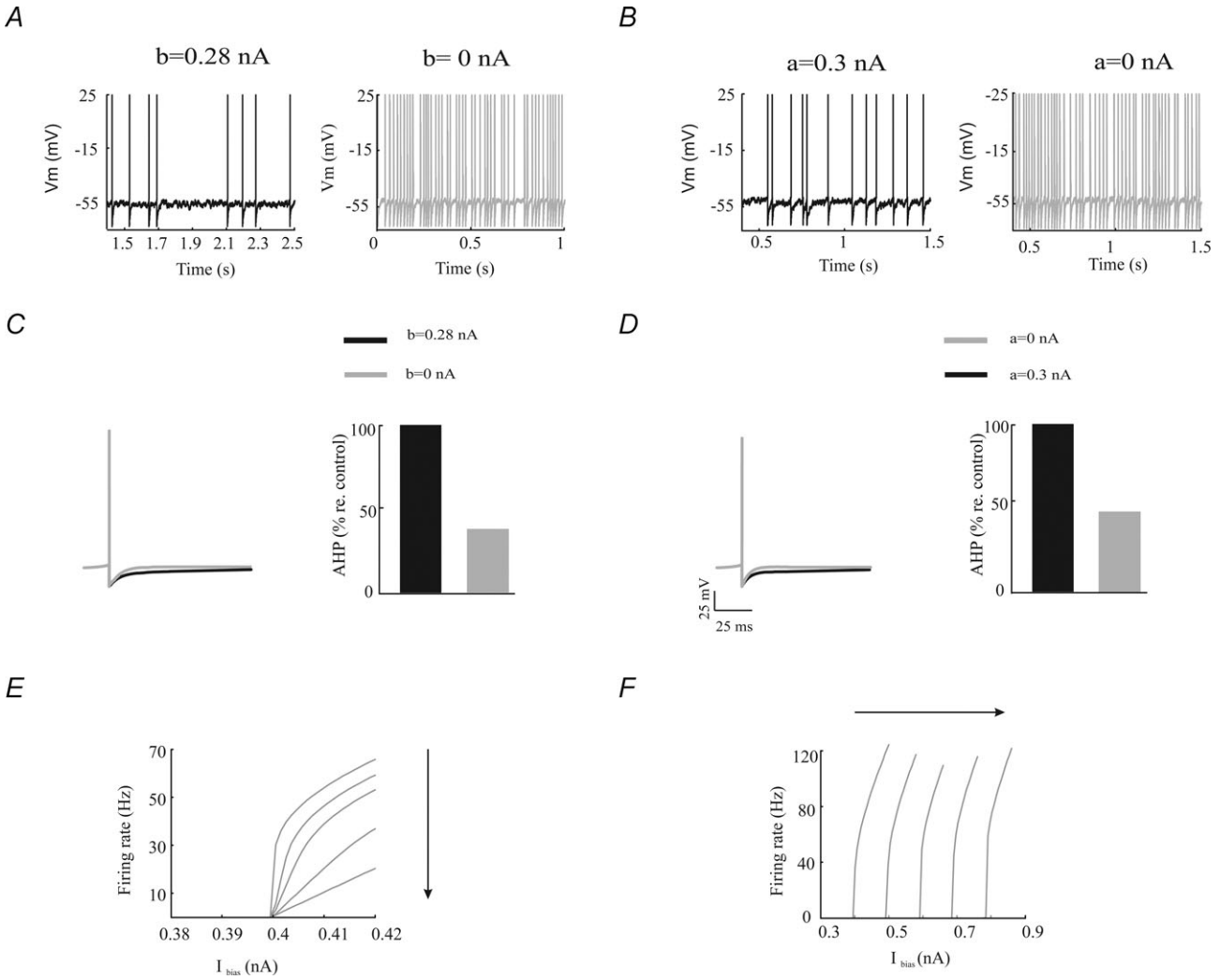


**Figure 5. A simple mathematical model reproduces the effects of UCL and XE-991 application on membrane excitability, burst firing, SFA, and the *f–I* curves**
*A*, model membrane potential trace under control conditions (left) and after removal of the spike-triggered adaptation current (right). *B*, model membrane potential trace under control conditions (left) and after removal of the subthreshold adaptation current (right). *C*, left, average action potential shapes under control (black) and after removal of the spike-triggered adaptation current (grey). Right, AHP size under control (black) and after removal of the spike-triggered adaptation current (grey). *D*, left, average action potential shapes under control (black) and after removal of the subthreshold adaptation current (grey). Right, AHP size under control (black) and after removal of the subthreshold adaptation current (grey). *E*, model *f–I* curves obtained from the model by increasing the spike-triggered adaptation gain *b*. Parameter values were the same as those used in Fig. 4*C*. The different curves were obtained with $b = 0$, 0.33, 0.67, 0.1 and 0.133 nA. *F*, model *f–I* curves obtained from the model by increasing the subthreshold adaptation gain *a*. Parameter values were the same as those used in Fig. 4*D*. The different curves were obtained with $a = 0$, 0.333, 0.667, 0.1 and 0.133 nA. Other parameters values were the same as those used for Fig. 4*C*.

the activation time constant $\tau_w$. To do so, we used approximations in our model neuron (see Methods). We found that, for low values of $\tau_w$, increasing the gain $a$ was equivalent to increasing the leak conductance $g_{leak}$. However, for high values of $\tau_w$, increasing $a$ was instead similar to decreasing the bias current $I_{bias}$. As such, we next computed the tuning index as a function of both the leak conductance $g_{leak}$ and the bias current $I_{bias}$. We found that increasing the leak conductance $g_{leak}$ decreased the tuning index for a fixed value of the bias current $I_{bias}$ (Fig. 9*A*). Increasing the bias current $I_{bias}$ for a fixed value of the leak conductance $g_{leak}$ also decreased the tuning index (Fig. 9*A*). Increasing the bias current $I_{bias}$ and decreasing the leak conductance $g_{leak}$ both increased firing rate (Fig. 9*B*).

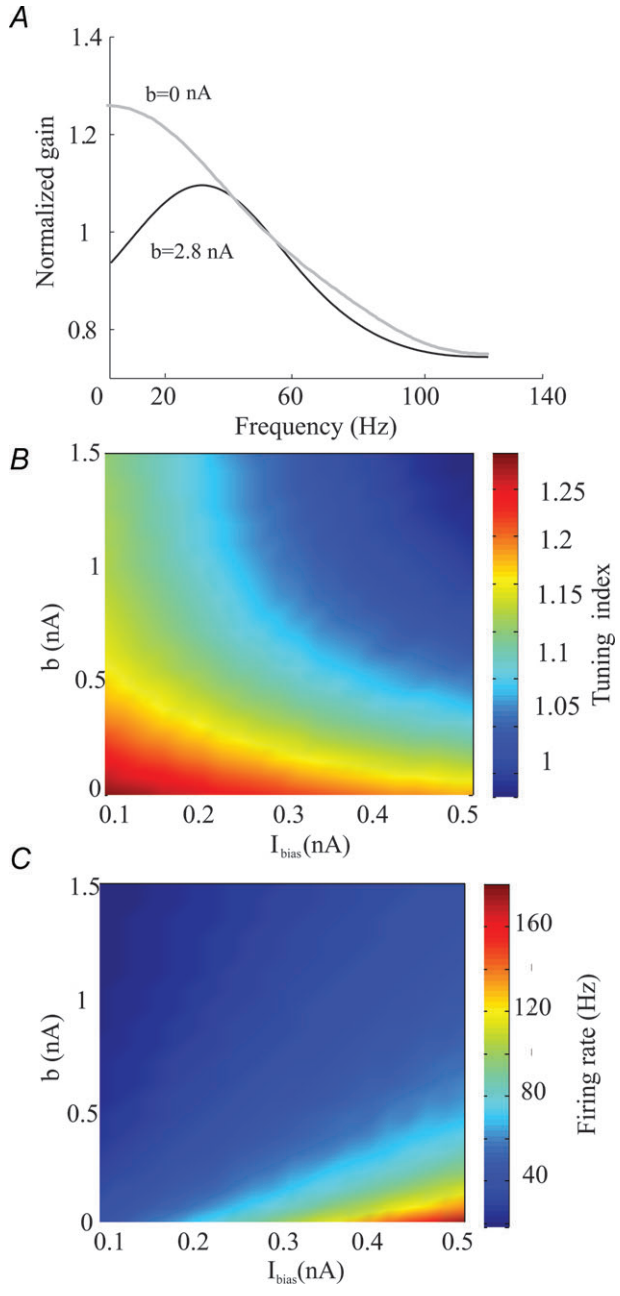


**Figure 6. Effects of the spike-triggered adaptation current on the neuronal transfer function**
*A*, gain curves with (black, $b = 0.3$ nA) and without (grey, $b = 0$ nA) the spike-triggered adaptation current. *B*, tuning index as a function of the bias current $I_{bias}$ and the spike-trigged adaptation gain. *C*, firing rate as a function of the bias current $I_{bias}$ and the spike-trigged adaptation gain $b$. Other parameters values were the same as those used for Fig. 4*C*.

These results can be understood in terms of neuronal transfer functions obtained in different regimes for our model as explored previously (Lindner *et al.* 2002; Brunel *et al.* 2003; Richardson *et al.* 2003). Indeed, most neuron models, including ours, behave as an integrator in the subthreshold regime (i.e. the regime for which the deterministic input is not sufficient to cause action potential firing) and as a resonator in the suprathreshold regime (i.e. the regime for which the deterministic input is sufficient to cause action potential firing). As such, increasing the bias current $I_{bias}$ or, equivalently, decreasing the subthreshold adaptation gain $a$ for large $\tau_w$, can cause a transition from the subthreshold regime where our model behaves like an integrator to the suprathreshold regime where our model behaves like a resonator (Richardson *et al.* 2003). Such a transition can have profound consequences on the shape of the neuronal transfer function (Lindner *et al.* 2002). Intuitively, for a neuron in the subthreshold regime, the probability of firing during a low frequency depolarization is increased as compared to a high frequency one because of the greater amount of time that the membrane potential is closer to the action potential threshold, giving rise to a low-pass tuning curve. In contrast, a neuron in the suprathreshold regime will tend to act like a resonator at a frequency equal to its mean firing rate. In that case, the transfer function will display a band-pass structure and peaks at a frequency roughly equal to the mean firing rate (Richardson *et al.* 2003; Schneider *et al.* 2011).

The effects of the subthreshold adaptation current on frequency tuning can thus be understood in terms of its effects on the subthreshold membrane conductance and the resting level of polarization. We propose that these effects can be mimicked by appropriate changes in the leak conductance $g_{leak}$ and the bias current $I_{bias}$, respectively. These changes are then dependent on the time constant $\tau_w$. Indeed, for high values of $\tau_w$, reducing the subthreshold adaptation gain $a$ is mostly equivalent to increasing the bias current $I_{bias}$, which can cause a transition from the subthreshold to the suprathreshold regime and therefore reduce tuning to low frequencies. In contrast, for low values of $\tau_w$, reducing the gain $a$ is mostly equivalent to decreasing the leak conductance $g_{leak}$ and actually increases tuning to low frequencies because this results in an increased membrane time constant (Fig. 8*A*). It is important to note that the changes in $g_{leak}$ and

$I_{bias}$ described will both increase firing rate (Fig. 8*B*). As such our modelling results provide an explanation for our initial experimental result that subthreshold and spike-triggered adaptation currents can have differential effects on frequency tuning.

**Blocking subthreshold adaptation currents results in a transition from the subthreshold to the suprathreshold regime in electrosensory pyramidal neurons.** If our model's prediction that blocking subthreshold adaptation currents causes a transition from the subthreshold

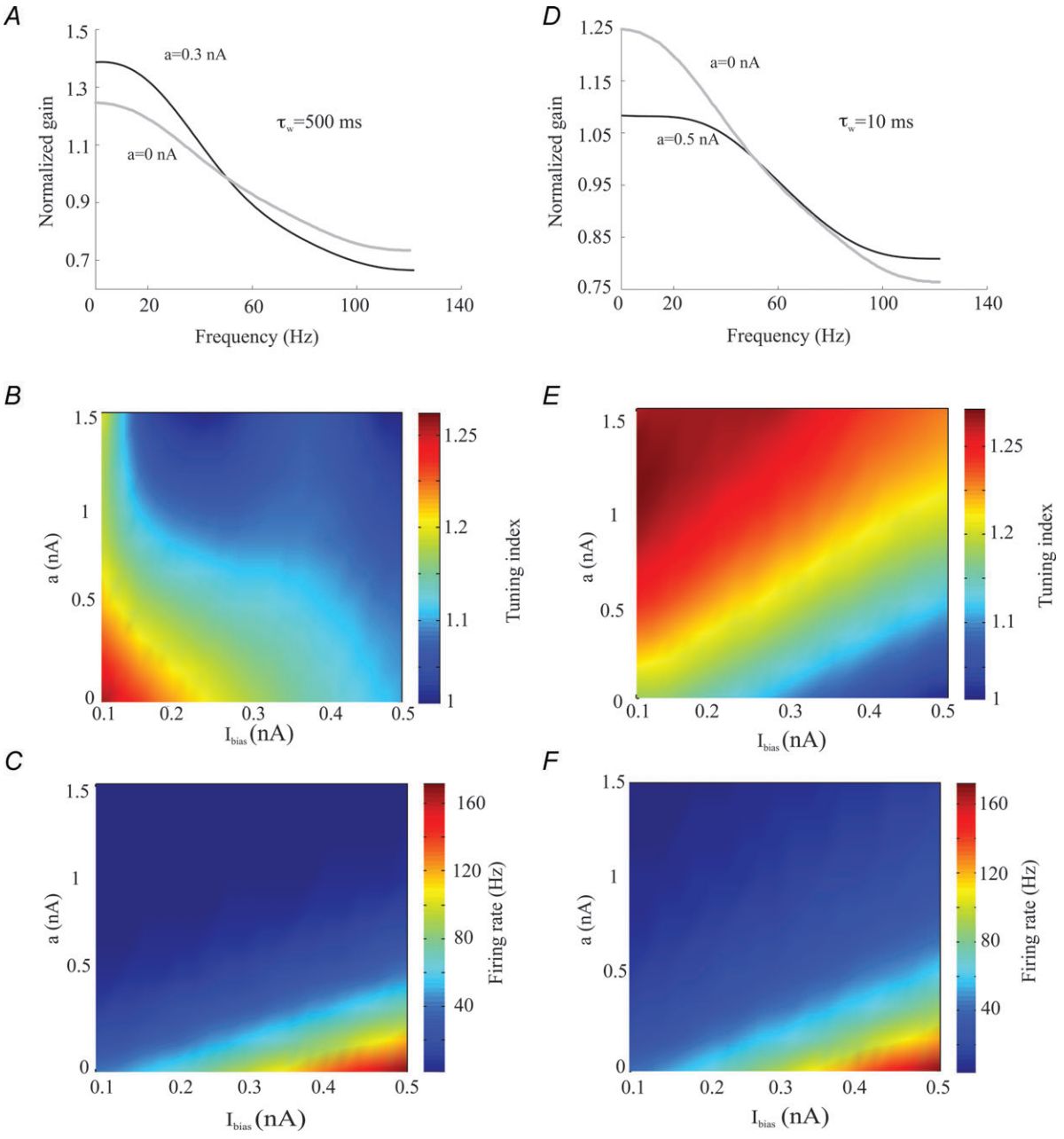


**Figure 7. Effects of subthreshold adaptation on the neuronal transfer function**
*A*, gain curves with (black, $a = 0.3$ nA) and without (grey, $a = 0$ nA) the subthreshold adaptation current for a high activation time constant ($\tau_w = 500$ ms). *B*, tuning index as a function of the bias current $I_{bias}$ and the subthreshold adaptation gain $a$ for high activation time constant. *C*, firing rate as a function of the bias current $I_{bias}$ and the subthreshold adaptation gain $a$ for high activation time constant. *D*, gain curves with (black, $a = 0.3$ nA) and without (grey, $a = 0$ nA) the subthreshold adaptation current for a low activation time constant ($\tau_w = 10$ ms). *E*, tuning index as a function of the bias current $I_{bias}$ and the subthreshold adaptation gain $a$ for low activation time constant. *F*, firing rate as a function of the bias current $I_{bias}$ and the subthreshold adaptation gain $a$ for low activation time constant. Other parameters values were the same as those used for Fig. 4*D*.

to suprathreshold regimes in electrosensory pyramidal neurons is correct, then we should see a relationship between the change in frequency for which the gain is maximal after XE-991 application and the change in the neuron's firing rate (Richardson *et al.* 2003). To test this prediction, we computed the change in the frequency at which gain was maximal as a function of the change in firing rate resulting from XE-991 application. We observed a strong and significant positive correlation between both quantities ($R = 0.6308$, $P = 0.01$, $n = 8$).

## Discussion

### Summary of results

We investigated the effects of UCL and XE-991 application on electrosensory pyramidal neuron responses. Both led to similar increases in excitability, decreases in the AHP, and increases in the adaptation time constant. However, we found that they led to opposite changes in the neuronal transfer function. Indeed, UCL application increased while XE-991 application instead decreased the response to low frequencies relative to that at high frequencies. To understand this surprising result, we built a mathematical model based on the integrate-and-fire formalism that included both subthreshold and spike-triggered adaptation currents. Despite its relative simplicity, this model successfully reproduced the effects of both UCL and XE-991 application on excitability and changes in the neuronal transfer function. However, we found that the effects of the subthreshold adaptation current on the neuronal transfer function were highly dependent on the value of the activation time constant. Indeed, for high values of the activation time constant, blocking the subthreshold adaptation current decreased the response to low frequencies relative to that at high frequencies, consistent with our experimental data. However, for low values of the activation time

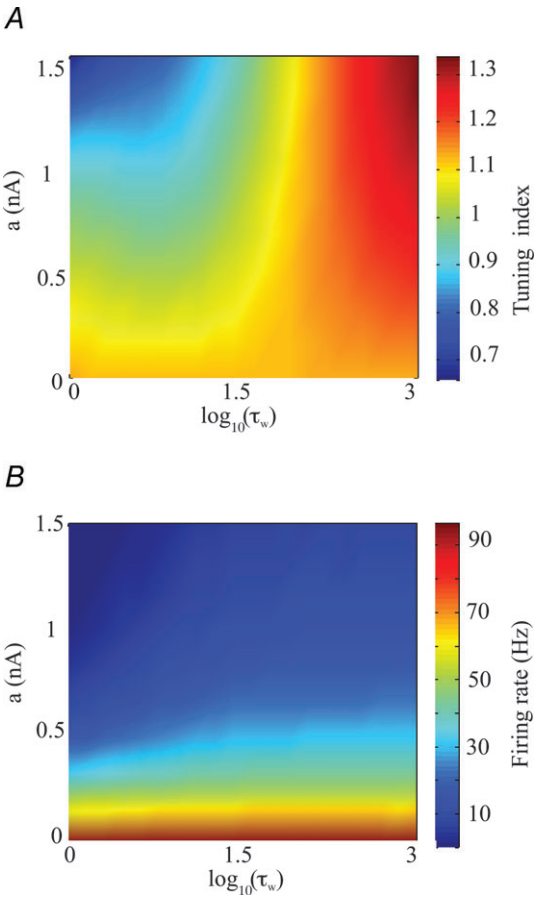


**Figure 8. Effects of the activation time constant $\tau_w$ on the neuronal transfer function**
*A*, tuning index as a function of the subthreshold adaptation gain *a* and the activation time constant $\tau_w$. *B*, firing rate as a function of the subthreshold adaptation gain *a* and the activation time constant $\tau_w$. Other parameters values were the same as those used for Fig. 4*D*.

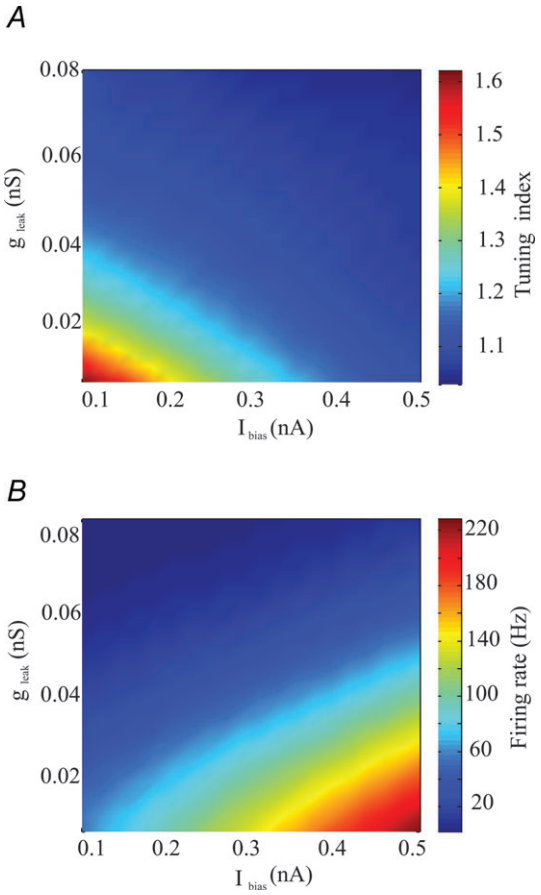


**Figure 9. Effects of the leak conductance $g_{leak}$ and bias current $I_{bias}$ on the neuronal transfer function**
*A*, tuning index as a function of the leak conductance $g_{leak}$ and the bias current $I_{bias}$. *B*, firing rate as a function of the leak conductance $g_{leak}$ and the bias current $I_{bias}$. Other parameters values were the same as those used for Fig. 4*C* except $b = 0$ nA.

constant, blocking the subthreshold adaptation current instead increased the response to low frequencies relative to that at high frequencies. We then used approximations to find that, for low values of the activation time constant, blocking the subthreshold adaptation current was equivalent to decreasing the leak conductance. Instead, for high values of the activation time constant, blocking the subthreshold adaptation current is instead equivalent to decreasing the bias current. Changes in these parameters can differentially affect the neuronal transfer function. In particular, decreasing the bias current can cause a transition from the suprathreshold to the subthreshold regime, which can have significant consequences on the neuronal transfer function.

### Adaptation and the neuronal transfer function

Several experimental studies have observed that spike frequency adaptation reduces and sometimes completely eliminates the response to the low frequency components of time varying stimuli (Nelson *et al.* 1997; French *et al.* 2001; Benda *et al.* 2005; Benda & Hennig, 2008). This is supported by theoretical studies that predict that adaptation will always suppress the neural response to frequencies lower than the inverse adaptation time constant relative to the response to frequencies greater than the inverse adaptation time constant (Benda & Herz, 2003). Our experimental results show that the effects of adaptation on the neuronal transfer function are instead highly dependent on the mechanisms that mediate adaptation. Indeed, while spike-triggered adaptation currents are predicted to have effects on the neuronal transfer function that are consistent with these predictions, our results suggest that the effects of subthreshold adaptation currents on the neuronal transfer function may or may not agree with these predictions depending on their activation time constant. This could explain recent experimental results showing that the effects of XE-991 on the neuronal transfer function are similar to those reported here (Guan *et al.* 2011).

### Role of subthreshold and spike-triggered adaptation currents in electrosensory processing

What are the roles played by subthreshold and spike-triggered adaptation currents in electrosensory processing? Answering this important question requires that we consider the applicability of our results under *in vivo* conditions. While it is clear that the intense synaptic bombardment to which electrosensory pyramidal neurons are subjected to under *in vivo* conditions can significantly alter their integration of synaptic input firing activity (Toporikova & Chacron, 2009; Avila Akerberg & Chacron, 2011), which is consistent with observations made in other systems (Destexhe *et al.* 2003; Schneider *et al.* 2011), *in vivo* conditions appear to have little effect on their neuronal transfer functions. This is because the neuronal transfer functions of electrosensory pyramidal neurons in response to current injection *in vitro* and in response to sensory stimulation *in vivo* are very similar (Krahe *et al.* 2008; Mehaffey *et al.* 2008*b*). This strongly suggests that the neuronal transfer function of electrosensory pyramidal neurons is mainly a function of intrinsic membrane properties.

Electrosensory pyramidal neurons display prominent SFA *in vivo* (Bastian *et al.* 2002; Krahe *et al.* 2008) and must also respond to behaviorally relevant stimuli whose temporal frequency content varies over a wide range (0–400 Hz) (Zupanc & Maler, 1993; Nelson & MacIver, 1999). Based on theoretical predictions (Benda & Herz, 2003), it is expected that pyramidal neurons would respond poorly to the low (<5 Hz) temporal frequency components of time varying stimuli as their adaptation time constants are greater than 20 ms (Krahe *et al.* 2008). However, *in vivo* studies have shown that electrosensory pyramidal neurons can respond strongly to frequencies as low as 1 Hz (Chacron *et al.* 2003*a*, 2005*a*; Krahe *et al.* 2008). Our results provide a potential solution to this contradiction as they show that subthreshold adaptation currents can promote increased tuning to low temporal frequencies while at the same time mediating SFA. As such, *in vivo* results support the notion that subthreshold adaptation currents are active in electrosensory pyramidal neurons and promote increased tuning to low frequencies, as predicted from our *in vitro* results. Moreover, our modelling results predict that these currents have slow activation time constants. Further studies performed *in vivo* are necessary to verify these predictions and are beyond the scope of this paper.

### Role of Subthreshold and spike-triggered adaptation currents in information processing in other systems

The role of subthreshold and spike-triggered adaptation currents in information processing continues to be of interest. Indeed, previous studies have suggested differential roles for each adaptation current (Ermentrout *et al.* 2001; Prescott & Sejnowski, 2008; Tabak *et al.* 2011). Our results are therefore consistent with these previous ones in that they predict differential roles for each current. However, one major difference is that previous studies have predicted that the differential effects of subthreshold and spike-triggered adaptation currents are mainly due to their differential activation properties (i.e. that the former is activated below the spiking threshold while the latter is only activated by spiking). Instead, our modelling results predict that it is their differential activation time constants that mediate their differential roles on the neuronal trans-

fer function. Previous studies performed in other systems have shown that subthreshold adaptation currents can have large (500 ms) (Prole *et al.* 2003; Regev *et al.* 2009) as well as small (10 ms) (Sogaard *et al.* 2001) activation time constants. As such, we predict that different subthreshold adaptation currents might have differential effects on frequency tuning. Further experiments are needed to test these predictions and are beyond the scope of this paper.

We note that the results presented in this study are likely to be applicable to other systems. This is in part due to the generic nature of the model used in this study. Indeed, this model has been used to successfully reproduce experimental data from other systems (Brette & Gerstner, 2005; Naud *et al.* 2008; Walcott *et al.* 2011). Moreover, SK channels which mediate spike-triggered adaptation currents in electrosensory pyramidal neurons system show over 90% functional homology with their mammalian counterparts (Ellis *et al.* 2008). Finally, previous studies have found that SK and M channels have effects on SFA and membrane excitability that are similar to those reported here (Smith *et al.* 2002; Greffrath *et al.* 2004; Stocker, 2004; Pedarzani *et al.* 2005; Waroux *et al.* 2005; Ellis *et al.* 2007*b*; Santini & Porter, 2010; but see Gu *et al.* 2008; Power & Sah, 2008; Vandecasteele *et al.* 2011).

### Adaptation and ambiguity

Spike frequency adaptation optimizes information transmission by rescaling the input–output relationship of neurons in response to changes in stimulus statistics (Adorjan *et al.* 1999; Muller *et al.* 1999; Brenner *et al.* 2000; Fairhall *et al.* 2001; Dragoi *et al.* 2002; Ulanovsky *et al.* 2003; Benda *et al.* 2005; Sharpee *et al.* 2006; Maravall *et al.* 2007). Further, by suppressing the response to the low frequency components of time varying stimuli, adaptation can make the response to the high frequency components invariant with respect to these (Barlow, 1961; Laughlin, 1989; Brenner *et al.* 2000; Wiskott, 2003; Gabbiani *et al.* 2004; Park *et al.* 2004; Benda & Hennig, 2008). While it is clear that such invariant representations are highly advantageous for an organism (e.g. to locate a given object independent of the level of light in a room), they can also introduce ambiguity in the neural code because the same neural response can then be elicited by different stimuli corresponding to different contexts (Fairhall *et al.* 2001; Wark *et al.* 2007).

Ideally, a given sensory system would transmit information about both a given stimulus feature and the context. One solution is to have parallel and independent transmission of both attributes as has been already observed in other contexts (Marr, 1982; Takahashi *et al.* 1984; Carr & Maler, 1986; Livingstone & Hubel, 1987; Merigan & Maunsell, 1993; Oertel, 1999; Gelfand, 2004; Bell & Maler, 2005; Kawasaki, 2005; McGillivray *et al.* 2012). Our results provide the first experimental evidence that a given sensory neuron can display spike frequency adaptation while still respond preferentially to the low frequency components of time varying stimuli. Therefore, our findings suggest that invariant representations of stimulus features can coexist with information about the context in which these features occur.

### Conclusion

We have shown that subthreshold and spike-triggered adaptation currents can differentially affect the neuronal transfer function. Our results thus provide a potential solution to the ambiguity in the neural code that can be caused by adaptation and suggest that parallel processing of stimulus features and context can occur in the central nervous system.

## References


Adams PR, Brown DA & Constanti A (1982). Pharmacological inhibition of the M-current. *J Physiol* **332**, 223–262.

Adorjan P, Piepenbrock C & Obermayer K (1999). Contrast adaptation and infomax in visual cortical neurons. *Rev Neurosci* **10**, 181–200.

Avila Akerberg O & Chacron MJ (2011). In vivo conditions influence the coding of stimulus features by bursts of action potentials. *J Comput Neurosci* **31**, 369–383.

Barlow HB (1961). Possible principles underlying the transformation of sensory messages. In *Sensory Communication*, ed. Rosenblith W. MIT Press, Cambridge, MA, USA.

Bastian J, Chacron MJ & Maler L (2002). Receptive field organization determines pyramidal cell stimulus-encoding capability and spatial stimulus selectivity. *J Neurosci* **22**, 4577–4590.

Bell C & Maler L (2005). Central neuroanatomy of electrosensory systems in fish. In *Electroreception*, ed. Bullock TH, Hopkins CD, Popper AN & Fay RR, pp. 68–111. Springer, New York.

Benda J & Hennig RM (2008). Spike-frequency adaptation generates intensity invariance in a primary auditory interneuron. *J Computat Neurosci* **24**, 113–136.

Benda J & Herz AV (2003). A universal model for spike-frequency adaptation. *Neural Computation* **15**, 2523–2564.

Benda J, Longtin A & Maler L (2005). Spike-frequency adaptation separates transient communication signals from background oscillations. *J Neurosci* **25**, 2312–2321.

Berman NJ & Maler L (1998). Distal versus proximal inhibitory shaping of feedback excitation in the electrosensory lateral line lobe: implications for sensory filtering. *J Neurophysiol* **80**, 3214–3232.

Borst A & Theunissen F (1999). Information theory and neural coding. *Nat Neurosci* **2**, 947–957.

Brenner N, Bialek W & de Ruyter van Steveninck R (2000). Adaptive rescaling maximizes information transmission. *Neuron* **26**, 695–702.

Brette R & Gerstner W (2005). Adaptive exponential integrate-and-fire model as an effective description of neuronal activity. *J Neurophysiol* **94**, 3637–3642.

Brunel N, Hakim V & Richardson MJ (2003). Firing-rate resonance in a generalized integrate-and-fire neuron with subthreshold resonance. *Phys Rev E Stat Nonlin Soft Matter Phys* **67**, 051916.

Carr CE & Maler L (1986). Electroreception in gymnotiform fish. Central anatomy and physiology. In *Electroreception*, ed. Bullock TH & Heiligenberg W, pp. 319–373. Wiley, New York.

Chacron MJ, Doiron B, Maler L, Longtin A & Bastian J (2003*a*). Non-classical receptive field mediates switch in a sensory neuron's frequency tuning. *Nature* **423**, 77–81.

Chacron MJ, Longtin A & Maler L (2001*a*). Negative interspike interval correlations increase the neuronal capacity for encoding time-varying stimuli. *J Neurosci* **21**, 5328–5343.

Chacron MJ, Longtin A & Maler L (2001*b*). Simple models of bursting and non-bursting electroreceptors. *Neurocomputing* **38**, 129–139.

Chacron MJ, Longtin A & Maler L (2003*b*). The effects of spontaneous activity, background noise, and the stimulus ensemble on information transfer in neurons. *Network* **14**, 803–824.

Chacron MJ, Longtin A & Maler L (2005*a*). Delayed excitatory and inhibitory feedback shape neural information transmission. *Phys Rev E Stat Nonlin Soft Matter Phys* **72**, 051917.

Chacron MJ, Longtin A & Maler L (2011). Efficient computation via sparse coding in electrosensory neural networks. *Curr Opin Neurobiol* **21**, 752–760.

Chacron MJ, Maler L & Bastian J (2005*b*). Electroreceptor neuron dynamics shape information transmission. *Nat Neurosci* **8**, 673–678.

Chance FS, Nelson SB & Abbott LF (1998). Synaptic depression and the temporal response characteristics of V1 cells. *J Neurosci* **18**, 4785–4799.

Deemyad T, Maler L & Chacron MJ (2011). Inhibition of SK and M channel mediated currents by 5-HT enables parallel processing by bursts and isolated spikes. *J Neurophysiol* **105**, 1276–1294.

Destexhe A, Rudolph M & Pare D (2003). The high-conductance state of neocortical neurons in vivo. *Nat Rev Neurosci* **4**, 739–751.

Dragoi V, Sharma J, Miller EK & Sur M (2002). Dynamics of neuronal sensitivity in visual cortex and local feature discrimination. *Nat Neurosci* **5**, 883–891.

Ellis LD, Krahe R, Bourque CW, Dunn RJ & Chacron MJ (2007*a*). Muscarinic receptors control frequency tuning through the downregulation of an A-type potassium current. *J Neurophysiol* **98**, 1526–1537.

Ellis LD, Maler L & Dunn RJ (2008). Differential distribution of SK channel subtypes in the brain of the weakly electric fish *Apteronotus leptorhynchus*. *J Com Neurol* **507**, 1964–1978.

Ellis LD, Mehaffey WH, Harvey-Girard E, Turner RW, Maler L & Dunn RJ (2007*b*). SK channels provide a novel mechanism for the control of frequency tuning in electrosensory neurons. *J Neurosci* **27**, 9491–9502.

Ermentrout B, Pascal M & Gutkin B (2001). The effects of spike frequency adaptation and negative feedback on the synchronization of neural oscillators. *Neural Comput* **13**, 1285–1310.

Faber ES & Sah P (2003). Calcium-activated potassium channels: multiple contributions to neuronal function. *Neuroscientist* **9**, 181–194.

Faber ESL & Sah P (2002). Physiological role of calcium-activated potassium currents in the rat lateral amygdala. *J Neurosci* **22**, 1618–1628.

Fairhall AL, Lewen GD, Bialek W & de Ruyter van Steveninck RR (2001). Efficiency and ambiguity in an adaptive neural code. *Nature* **412**, 787–792.

French AS, Hoger U, Sekizawa S & Torkkeli PH (2001). Frequency response functions and information capacities of paired spider mechanoreceptor neurons. *Biol Cybern* **85**, 293–300.

Fuhrmann G, Segev I, Markram H & Tsodyks M (2002). Coding of temporal information by activity-dependent synapses. *J Neurophysiol* **87**, 140–148.

Gabbiani F, Krapp HG, Hatsopoulos N, Mo CH, Koch C & Laurent G (2004). Multiplication and stimulus invariance in a looming-sensitive neuron. *J Physiol (Paris)* **98**, 19–34.

Gelfand S (2004). *Hearing: An Introduction to Psychological and Physiological Acoustics*. Informa Healthcare, Colchester.

Glantz RM & Schroeter JP (2004). Analysis and simulation of gain control and precision in crayfish visual interneurons. *J Neurophysiol* **92**, 2747–2761.

Greffrath W, Magerl W, Disque-Kaiser U, Martin E, Reuss S & Boehmer G (2004). Contribution of $Ca^{2+}$-activated $K^+$ channels to hyperpolarizing after-potentials and discharge pattern in rat supraoptic neurones. *J Neuroendocrinol* **16**, 577–588.

Gu N, Hu H, Vervaeke K & Storm JF (2008). SK (KCa2) channels do not control somatic excitability in CA1 pyramidal neurons but can be activated by dendritic excitatory synapses and regulate their impact. *J Neurophysiol* **100**, 2589–2604.

Guan D, Higgs MH, Horton LR, Spain WJ & Foehring RC (2011). Contributions of Kv7-mediated potassium current to sub- and suprathreshold responses of rat layer II/III neocortical pyramidal neurons. *J Neurophysiol* **106**, 1722–1733.

Halliwell JV & Adams PR (1982). Voltage-clamp analysis of muscarinic excitation in hippocampal neurons. *Brain research* **250**, 71–92.

Hallworth NE, Wilson CJ & Bevan MD (2003). Apamin-sensitive small conductance calcium-activated potassium channels, through their selective coupling to voltage-gated calcium channels, are critical determinants of the precision, pace, and pattern of action potential generation in rat subthalamic nucleus neurons in vitro. *J Neurosci* **23**, 7525–7542.

Hitschfeld ÉM, Stamper SA, Vonderschen K, Fortune ES & Chacron MJ (2009). Effects of restraint and immobilization on electrosensory behaviors of weakly electric fish. *ILAR J* **50**, 361–372.

Kawasaki M (2005). Central neuroanatomy of electrosensory systems in fish. In *Electroreception*, ed. Bullock TH, Hopkins CD, Popper AN & Fay RR, pp. 154–194. Springer, New York.

Koyama S & Appel SB (2006). Characterization of M-current in ventral tegmental area dopamine neurons. *J Neurophysiol* **96**, 535–543.

Krahe R, Bastian J & Chacron MJ (2008). Temporal processing across multiple topographic maps in the electrosensory system. *J Neurophysiol* **100**, 852–867.

Laughlin SB (1989). The role of sensory adaptation in the retina. *J Exp Biol* **146**, 39–62.

Lindner B, Gangloff D, Longtin A & Lewis JE (2009). Broadband coding with dynamic synapses. *J Neurosci* **29**, 2076–2087.

Lindner B, Schimansky-Geier L & Longtin A (2002). Maximizing spike train coherence or incoherence in the leaky integrate-and-fire model. *Phys Rev E Stat Nonlin Soft Matter Phys* **66**, 031916.

Livingstone MS & Hubel DH (1987). Psychophysical evidence for separate channels for the perception of form, color, movement, and depth. *J Neurosci* **7**, 3416–3468.

Madamba SG, Schweitzer P & Siggins GR (1999). Dynorphin selectively augments the M-current in hippocampal CA1 neurons by an opiate receptor mechanism. *J Neurophysiol* **82**, 1768–1775.

Maler L (1979). The posterior lateral line lobe of certain gymnotiform fish. Quantitative light microscopy. *J Comp Neurol* **183**, 323–363.

Maler L (2009). Receptive field organization across multiple electrosensory maps. I. Columnar organization and estimation of receptive field size. *J Comp Neurol* **516**, 376–393.

Maler L, Sas EK & Rogers J (1981). The cytology of the posterior lateral line lobe of high frequency weakly electric fish (Gymnotidae): Differentiation and synaptic specificity in a simple cortex. *J Comp Neurol* **195**, 87–139.

Maravall M, Petersen RS, Fairhall AL, Arabzadeh E & Diamond ME (2007). Shifts in coding properties and maintenance of information transmission during adaptation in barrel cortex. *PLoS Biol* **5**, e19.

Marr D (1982). *Vision*. Freeman, New York.

Mathieson WB & Maler L (1988). Morphological and electrophysiological properties of a novel *in vitro* preparation: the electrosensory lateral line lobe brain slice. *J Comp Physiol A* **163**, 489–506.

McGillivray P, Vonderschen K, Fortune ES & Chacron MJ (2012). Parallel coding of first and second order stimulus attributes by midbrain electrosensory neurons. *J Neurosci* **32**, 5510–5524.

Mehaffey WH, Doiron B, Maler L & Turner RW (2005). Deterministic multiplicative gain control with active dendrites. *J Neurosci* **25**, 9968–9977.

Mehaffey WH, Ellis LD, Krahe R, Dunn RJ & Chacron MJ (2008*a*). Ionic and neuromodulatory regulation of burst discharge controls frequency tuning. *J Physiol (Paris)* **102**, 195–208.

Mehaffey WH, Maler L & Turner RW (2008*b*). Intrinsic frequency tuning in ELL pyramidal cells varies across electrosensory maps. *J Neurophysiol* **99**, 2641–2655.

Merigan WH & Maunsell JH (1993). How parallel are the primate visual pathways? *Annu Rev Neurosci* **16**, 369–402.

Muller JR, Metha AB, Krauskopf J & Lennie P (1999). Rapid adaptation in visual cortex to the structure of images. *Science* **285**, 1405–1408.

Naud R, Marcille N, Clopath C & Gerstner W (2008). Firing patterns in the adaptive exponential integrate-and-fire model. *Biol Cybernet* **99**, 335–347.

Nelson ME & MacIver MA (1999). Prey capture in the weakly electric fish *Apteronotus albifrons*: sensory acquisition strategies and electrosensory consequences. *J Exp Biol* **202**, 1195–1203.

Nelson ME, Xu Z & Payne JR (1997). Characterization and modeling of P-type electrosensory afferent responses to amplitude modulations in a wave-type electric fish. *J Comp Physiol A* **181**, 532–544.

Oertel D (1999). The role of timing in the brain stem auditory nuclei of vertebrates. *Annu Rev Physiol* **61**, 497–519.

Oswald AMM, Chacron MJ, Doiron B, Bastian J & Maler L (2004). Parallel processing of sensory input by bursts and isolated spikes. *J Neurosci* **24**, 4351–4362.

Park TJ, Klug A, Holinstat M & Grothe B (2004). Interaural level difference processing in the lateral superior olive and the inferior colliculus. *J Neurophysiol* **92**, 289–301.

Pedarzani P, McCutcheon JE, Rogge G, Jensen BS, Christophersen P, Hougaard C, Strobaek D & Stocker M (2005). Specific enhancement of SK channel activity selectively potentiates the afterhyperpolarizing current $I_{AHP}$ and modulates the firing properties of hippocampal pyramidal neurons. *J Biol Chem* **280**, 41404–41411.

Peron S & Gabbiani F (2009*a*). Spike frequency adaptation mediates looming stimulus selectivity in a collision-detecting neuron. *Nat Neurosci* **12**, 318–326.

Peron SP & Gabbiani F (2009*b*). Role of spike-frequency adaptation in shaping neuronal response to dynamic stimuli. *Biol Cybernet* **100**, 505–520.

Power JM & Sah P (2008). Competition between calcium-activated $K^+$ channels determines cholinergic action on firing properties of basolateral amygdala projection neurons. *J Neurosci* **28**, 3209–3220.

Prescott SA & Sejnowski TJ (2008). Spike-rate coding and spike-time coding are affected oppositely by different adaptation mechanisms. *J Neurosci* **28**, 13649–13661.

Prole DL, Lima PA & Marrion NV (2003). Mechanisms underlying modulation of neuronal KCNQ2/KCNQ3 potassium channels by extracellular protons. *J Gen Physiol* **122**, 775–793.

Regev N, Degani-Katzav N, Korngreen A, Etzioni A, Siloni S, Alaimo A, Chikvashvili D, Villarroel A, Attali B & Lotan I (2009). Selective interaction of syntaxin 1A with KCNQ2: possible implications for specific modulation of presynaptic activity. *PLoS One* **4**, e6586.

Richardson MJ, Brunel N & Hakim V (2003). From subthreshold to firing-rate resonance. *J Neurophysiol* **89**, 2538–2554.

Rieke F, Warland D, de Ruyter van Steveninck RR & Bialek W (1996). *Spikes: Exploring the Neural Code*. MIT Press, Cambridge, MA, USA.

Sadeghi SG, Chacron MJ, Taylor MC & Cullen KE (2007). Neural variability, detection thresholds, and information transmission in the vestibular system. *J Neurosci* **27**, 771–781.

Sah P & Faber ES (2002). Channels underlying neuronal calcium-activated potassium currents. *Prog Neurobiol* **66**, 345–353.

Santini E & Porter JT (2010). M-type potassium channels modulate the intrinsic excitability of infralimbic neurons and regulate fear expression and extinction. *J Neurosci* **30**, 12379–12386.

Schneider AD, Cullen KE & Chacron MJ (2011). In vivo conditions induce faithful encoding of stimuli by reducing nonlinear synchronization in vestibular sensory neurons. *PLoS Comp Biol* **7**, e1002120.

Shah MM, Mistry M, Marsh SJ, Brown DA & Delmas P (2002). Molecular correlates of the M-current in cultured rat hippocampal neurons. *J Physiol* **544**, 29–37.

Sharpee TO, Sugihara H, Kurgansky AV, Rebrik SP, Stryker MP & Miller KD (2006). Adaptive filtering enhances information transmission in visual cortex. *Nature* **439**, 936–942.

Smith MR, Nelson AB & Du Lac S (2002). Regulation of firing response gain by calcium-dependent mechanisms in vestibular nucleus neurons. *J Neurophysiol* **87**, 2031–2042.

Sobel EC & Tank DW (1994). In vivo $Ca^{2+}$ dynamics in a cricket auditory neuron: an example of chemical computation. *Science* **263**, 823–826.

Sogaard R, Ljungstrom T, Pedersen KA, Olesen SP & Jensen BS (2001). KCNQ4 channels expressed in mammalian cells: functional characteristics and pharmacology. *Am J Physiol Heart Circ Physiol* **280**, C859–866.

Stamper SA, Carrera GE, Tan EW, Fugere V, Krahe R & Fortune ES (2010). Species differences in group size and electrosensory interference in weakly electric fishes: implications for electrosensory processing. *Behav Brain Res* **207**, 368–376.

Stocker M (2004). $Ca^{2+}$-activated $K^+$ channels: molecular determinants and function of the sk family. *Nat Rev Neurosci* **5**, 758–770.

Tabak J, Rinzel J & Bertram R (2011). Quantifying the relative contributions of divisive and subtractive feedback to rhythm generation. *PLoS Comp Biol* **7**, e1001124.

Takahashi T, Moiseff A & Konishi M (1984). Time and intensity cues are processed independently in the auditory system of the owl. *J Neurosci* **4**, 1781–1786.

Tan EW, Nizar JM, Carrera GE & Fortune ES (2005). Electrosensory interference in naturally occurring aggregates of a species of weakly electric fish, Eigenmannia virescens. *Behav Brain Res* **164**, 83–92.

Toporikova N & Chacron MJ (2009). Dendritic SK channels gate information processing *in vivo* by regulating an intrinsic bursting mechanism seen *in vitro*. *J Neurophysiol* **102**, 2273–2287.

Ulanovsky N, Las L & Nelken I (2003). Processing of low-probability sounds by cortical neurons. *Nat Neurosci* **6**, 391–398.

Vandecasteele M, Deniau JM & Venance L (2011). Spike frequency adaptation is developmentally regulated in substantia nigra pars compacta dopaminergic neurons. *Neuroscience* **192**, 1–10.

Wainwright ML, Zhang H, Byrne JH & Cleary LJ (2002). Localized neuronal outgrowth induced by long-term sensitization training in aplysia. *J Neurosci* **22**, 4132–4141.

Walcott EC, Higgins EA & Desai NS (2011). Synaptic and intrinsic balancing during postnatal development in rat pups exposed to valproic acid in utero. *J Neurosci* **31**, 13097–13109.

Wang XJ (1998). Calcium coding and adaptive temporal computation in cortical pyramidal neurons. *J Neurophysiol* **79**, 1549–1566.

Wark B, Lundstrom BN & Fairhall A (2007). Sensory adaptation. *Curr Opin Neurobiol* **17**, 423–429.

Waroux O, Massotte L, Alleva L, Graulich A, Thomas E, Liegeois JF, Scuvee-Moreau J & Seutin V (2005). SK channels control the firing pattern of midbrain dopaminergic neurons in vivo. *Eur J Neurosci* **22**, 3111–3121.

Williams S, Serafin M, Muhlethaler M & Bernheim L (1997). Distinct contributions of high- and low-voltage-activated calcium currents to afterhyperpolarizations in cholinergic nucleus basalis neurons of the guinea pig. *J Neurosci* **17**, 7307–7315.

Wiskott L (2003). Slow feature analysis: a theoretical analysis of optimal free responses. *Neural Comput* **15**, 2147–2177.

Yue C & Yaari Y (2004). KCNQ/M channels control spike afterdepolarization and burst generation in hippocampal neurons. *J Neurosci* **24**, 4614–4624.

Zupanc GKH & Maler L (1993). Evoked chirping in the weakly electric fish *Apteronotus leptorhynchus*: a quantitative biophysical analysis. *Can J Zool* **71**, 2301–2310.

## Author contributions

The experiments were performed by T.D. at the Department of Physiology, McGill University. The modelling was performed by J.K. and M.J.C. at the Department of Physiology, McGill University. Analysis, interpretation of results and manuscript writing: T.D., J.K. Study concept, manuscript editing and critical revision for intellectual content: M.J.C. All authors approved the final version of the manuscript.

## Acknowledgements

We thank Drs Kathleen Cullen, Charles Bourque and Soroush Sadeghi for useful comments on the manuscript. This research was supported by CIHR, FQRNT, CFI and CRC (M.J.C.).